



U.S. DEPARTMENT OF
ENERGY

PNNL-19119

Prepared for the
U.S. Nuclear Regulatory Commission
under a Related Services Agreement
with the U.S. Department of Energy
Contract DE-AC05-76RL01830

Preliminary Examination of Cracks in Alloy 152, 52, and 52M Weld Metals

MB Toloczko
MJ Olszta

RJ Seffens
SM Bruemmer

January 2010



Pacific Northwest
NATIONAL LABORATORY

*Proudly Operated by **Battelle** Since 1965*

DISCLAIMER

This report was prepared as an account of work sponsored by an agency of the United States Government. Neither the United States Government nor any agency thereof, nor Battelle Memorial Institute, nor any of their employees, makes **any warranty, express or implied, or assumes any legal liability or responsibility for the accuracy, completeness, or usefulness of any information, apparatus, product, or process disclosed, or represents that its use would not infringe privately owned rights.** Reference herein to any specific commercial product, process, or service by trade name, trademark, manufacturer, or otherwise does not necessarily constitute or imply its endorsement, recommendation, or favoring by the United States Government or any agency thereof, or Battelle Memorial Institute. The views and opinions of authors expressed herein do not necessarily state or reflect those of the United States Government or any agency thereof.

PACIFIC NORTHWEST NATIONAL LABORATORY

operated by

BATTELLE

for the

UNITED STATES DEPARTMENT OF ENERGY

under Contract DE-AC05-76RL01830



This document was printed on recycled paper.

(9/2003)

Preliminary Examination of Cracks in Alloy 152, 52, and 52M Weld Metals

MB Toloczko
MJ Olszta

RJ Seffens
SM Bruemmer

January 2010

Prepared for
U.S. Nuclear Regulatory Commission
under a Related Services Agreement
with the U.S. Department of Energy
Contract DE-AC05-76RL01830
NRC Project JCN N6547

Pacific Northwest National Laboratory
Richland, Washington 99352

Summary

The primary goal of these initial examinations was to assess defects in prototypic, industry-produced, Alloy 52, 52M, and 152 mockup welds. Weld metals were characterized in three different mockup configurations: (1) Alloy 52 and 152 U-groove weld mockups both made by MHI, (2) an Alloy 52M overlay made by Ringhals AB, and (3) an Alloy 52M inlay mockup also made by Ringhals AB. The only significant defects identified within the Alloy 52, 52M, or 152 welds were intergranular cracks. No evidence for other weld defects was found. The optical appearance of the weld cracks did not vary significantly between the four different mockups with crack openings varying from less than 1 μm (almost invisible) to approximately 10 μm . Short cracks appear to have approximately the same amount of crack opening as the longer cracks. It is possible that shorter or tighter cracks may have been present but were obscured and difficult to identify with the preparation method used.

General differences were observed in both the location and density of cracks among the various welds. The fewest cracks were identified in the Alloy 152 weld metal, either in the butter layers or the fill. A sharp macroscopic crack in the Alloy 152 was present at the base of the U-groove weld extending from the Type 304SS plate and butter butt joint. Even for this high-stress location, only a single secondary crack was present in this region. The two other confirmed weld cracks in the Alloy 152 U-groove mockup were near the top of the weld and near the butter interface off to one side of the weld, respectively. Therefore, the Alloy 152 weld was quite resistant to the formation of weld cracks whether due to the weld metal composition or to the welding procedure or both.

The Alloy 52 U-groove mockup revealed a substantial amount of weld cracks clustered around the main macroscopic crack that ran up into the fill weld from the 304SS plate and butter butt joint. This main crack was much more open than seen in the Alloy 152 weld indicating much higher local stresses. Although this local region showed a high density of cracks, it is important to note that no other cracks were found in the Alloy 52 weld. As a result, the Alloy 52 in this U-groove weld also appears to be resistant to the formation of cracks except in the high-stress region created above the plate butt joint.

The greatest number of weld cracks was found in the Alloy 52M overlay. They were clustered in three local regions. It is uncertain whether this distribution is random or due to differences in the weld wire or practice local to these regions. Because the Alloy 52M layer was robotically welded, one would expect the welding parameters to have remained constant. The majority of the weld cracks appeared to be randomly placed in each of the three sections, but there were many small weld cracks associated with the first Alloy 52M weld pass near the Alloy 690 interface. These results suggest that this Alloy 52M weld metal is more susceptible to the formation of intergranular cracks during in the application of the first weld pass.

The final mockup examined was the Alloy 52M inlay. Most of the weld cracks were found near the final Alloy 52M weld pass in this rather thick inlay. Only isolated cracks were identified near the Alloy 52M–Alloy 82 interface, and nearly all of these were in the Alloy 82 material. The weld cracks in the Alloy 52M were typically less than 100 μm in length, but there was one possible instance of an approximately 500- μm crack in the final weld pass.

The preliminary weld crack examinations reported here indicate that small intergranular weld cracks will be present in most Alloy 52, 52M, and 152 weldments. Brief comments can be made on implications to the use of thin, high-Cr overlays or inlays to provide corrosion resistance. The observed cracks do not appear to provide a continuous path for water to reach the more stress corrosion cracking (SCC) susceptible, lower-Cr Alloy 182 or 82 weld metal. While the typical crack size in all the welds was 100 μm or less, in three of the weld mockups, several 500- μm -long cracks were observed. This length is insufficient for a single crack to span even a thin overlay, but a clustering of interconnected cracks may potentially provide a path. This seems unlikely based on the current limited results; however, more detailed studies of crack size and three-dimensional distributions would need to be performed to better assess the probability that such interconnected cracks could exist.

More important is the question whether these pre-existing flaws can act as sites for accelerated crack growth during LWR service. The location and length of a weld crack in the inlay or overlay would obviously have a strong affect on the local stress intensities. A long weld crack that intersects the surface of an inlay or overlay would be subject to higher fatigue-driven stresses and clusters of cracks could more easily become interconnected. Similar issues can be envisioned for a weld crack on the surface acting as a nucleation site for the growth of an SCC crack. Measured SCC propagation rates of these materials are extremely slow, with perhaps a maximum rate of approximately 0.1 mm/year at relatively high stress intensity values. It would take roughly 20 years for an SCC crack to span a 2-mm-thick inlay repair. A final key issue is whether the microstructure and microchemistry in the regions of weld cracks are inherently more susceptible to SCC. This could result from local deformation-induced structures, segregation-induced microchemistries, or second-phase precipitation particularly associated with grain boundaries where pre-existing cracks are present. Focused SCC testing should be performed to evaluate such microstructural and microchemical variations in candidate inlay and overlay materials.

Acronyms and Abbreviations

ATEM	analytical transmission electron microscopy
BSE	backscattered electron
BWR	boiling-water reactor
CGR	crack-growth rate
EBSD	electron backscatter diffraction
EDS	energy dispersive x-ray spectroscopy
EPRI	Electric Power Research Institute
GTAW	gas tungsten arc welding
HAZ	heat-affected-zone
ID	identification
IG	intergranular
IPF	inverse pole figure
LWR	light-water reactor
μm	micrometer
NRC	U.S. Nuclear Regulatory Commission
PWR	pressurized-water reactor
PWSCC	primary water stress corrosion cracking
SCC	stress-corrosion cracking
SEM	scanning electron microscopy
SMAW	shielded metal arc welding
SS	stainless steel
TEM	transmission electron microscopy

Contents

Summary	iii
Acronyms and Abbreviations	v
1.0 Background and Research Scope.....	1.1
2.0 Materials.....	2.1
2.1 MHI Alloy 52 and 152 Weld Mockups.....	2.1
2.2 Ringhals Alloy 52M/182 Overlay and Alloy 52M/82 Inlay Mockups.....	2.3
3.0 Metallographic Weld Defect Characterizations.....	3.1
3.1 Alloy 152 Weld Mockup.....	3.1
3.2 Alloy 52 Weld Mockup.....	3.5
3.3 Alloy 52M/182 Overlay Mockup.....	3.8
3.4 Alloy 52M/82 Inlay Mockup.....	3.13
4.0 Analytical Electron Microscopy Characterization of Weld Mockups.....	4.1
4.1 SEM and EBSD of the Ringhals Alloy 52M/82 Inlay Mockup	4.1
4.2 SEM and EBSD of MHI Alloy 52 U-Groove Weld Mockup	4.3
4.3 SEM and TEM of Weld Cracks in Alloy 52 – 304SS Overlay Mockup.....	4.7
4.4 SEM of MHI Alloy 152 Weld Mockup.....	4.16
5.0 Summary of Preliminary Results.....	5.1

Figures

2.1	Optical Images of MHI Alloy 52 and Alloy 152 Weld Mockups Showing U-groove Weld in Cross Section	2.2
2.2	Sketch Showing the Relative Location of Slices Taken from the MHI Alloy 152 Mockup.....	2.2
2.3	Overview of the Ringhals Alloy 52M Overlay Mockup where Alloy 52M was Robotically Welded to an Alloy 690 Plate Followed by Alloy 182 Manually Welded onto the Alloy 52M.....	2.3
2.4	Overview of the Ringhals Alloy 52M Inlay Mockup	2.4
2.5	Side View of Ringhals Alloy 52M Mockup Showing Cut Lines for CT Specimen Blanks and Metallography Slices.....	2.4
3.1	Overview Image of the Alloy 152 Weld Slice B with areas Showing Possible Weld Defects Highlighted by the Green Boxes.....	3.2
3.2	Optical Metallographs Illustrating Regions in the Alloy 152 Weld Metal Slice B.....	3.2
3.3	Optical Metallographs Illustrating Regions in the Alloy 152 Weld Metal Slice B.....	3.3
3.4	Overview Image of the Alloy 152 Weld Slice F with Areas Showing Possible Weld Defects Highlighted by the Green Boxes.....	3.3
3.5	Optical Metallographs Illustrating Regions in the Alloy 152 Weld Metal Slice F.....	3.4
3.6	Overview Image of the Alloy 152 Weld Slice X.....	3.4
3.7	Overview Image of the Alloy 52 Slice Showing Large Separation and Cracking Extending Up from the Butt Joint at the Bottom of the U-groove	3.5
3.8	Weld Cracks in Alloy 52 Weld Metal Adjacent to Main Crack as Illustrated in Figure 3.7	3.6
3.9	Etched Weld Microstructure is Shown to Illustrate the Typical Morphology of the Cracks in the MHI Alloy 52 Weld Metal.....	3.7
3.10	Overview Image of the Alloy 52M – Alloy 182 Overlay Slice A Showing the Alloy 690, Alloy 52M, and Alloy 182 Layers Along with Selected Regions of Analysis	3.8
3.11	Optical Metallographs Illustrating Regions in the Alloy 52M Overlay Slice A Containing Weld Cracks.....	3.9
3.12	Overview Image of the Alloy 52M – Alloy 182 Overlay Slice B Showing Selected Regions of Analysis	3.9
3.13	Optical Metallographs Illustrating Regions in the Alloy 52M Overlay Slice B Containing Weld Cracks.....	3.10
3.14	Etched Weld Microstructure is Shown to Illustrate the Typical Morphology of the Cracks in the Alloy 52M Overlay	3.11
3.15	Etched Weld Microstructure is Shown to Illustrate the Typical Morphology of the Cracks in the Alloy 52M Overlay	3.12
3.16	Overview Image of the Alloy 52M Inlay Mockup Slice A Showing the Low-Alloy Steel, Alloy 82, Alloy 52M and Alloy 152 Layers Along with Selected Regions of Analysis	3.13
3.17	Optical Metallograph Illustrating a Region in the Alloy 52M Inlay Slice A Containing Small Pits Probably Resulting from Particle Pullout during Polishing.....	3.14
3.18	Overview Image of the Alloy 52M Inlay Mockup Slice B Showing the Low-Alloy Steel, Alloy 82, Alloy 52M and Alloy 152 Layers Along with Selected Regions of Analysis	3.15

3.19	Optical Metallographs Illustrating Regions in the Ringhals Alloy 52M Inlay Mockup Slice B Containing Small Weld Cracks in the Alloy 52M Weld Metal.....	3.16
3.20	Overview Image of the Ringhals Inlay Mockup Slice C Showing Regions Where Indications of Weld Cracks were Observed and Analyzed.....	3.17
3.21	Two Examples of Weld Cracks Found in Ringhals Inlay Mockup Slice C.....	3.17
4.1	EBSD Pattern Quality and IPF-Z Images of a Weld Crack in the Ringhals Alloy 52M Inlay (C-6) Showing Weld Metal Microstructure, Crack Morphology, and Areas of Deformation.....	4.1
4.2	SEM-BSE Image and EDS Maps of the Ringhals Alloy 52M Inlay Weld (C-6) Revealing Significant Compositional Variations within Grains Particularly for Nb.....	4.2
4.3	EBSD Pattern Quality Images of Three Regions of Cracks in the MHI Alloy 52 U-Groove Weld Where EBSD Characterization was Performed.....	4.3
4.4	EBSD IPF-Z Illustrating the Differences in Grain Orientations and Deformation in the Vicinity of the MHI Alloy 52 U-groove Weld Cracks.....	4.4
4.5	EBSD IPF-Y Image Illustrating Differences in Grain Orientation and Rotation Around Weld Cracks that Formed Along High-Energy Grain Boundaries in the MHI Alloy 52 U-groove Weld.....	4.5
4.6	EBSD IPF-Y Image of the MHI Alloy 52 U-groove Weld Illustrating Differences in Grain Orientation and Deformation Near Weld Cracks Situated Along High-Energy Grain Boundaries and Regions of Fine Grains.....	4.6
4.7	SEM-EDS Maps of the MHI Alloy 52 U-groove Mockup Show Very Little Variation in Elemental Composition with the Weld Cracks.....	4.6
4.8	Optical Micrographs Provided by Ringhals Showing an Alloy 52 Weld Metal Overlay on a 304SS Housing.....	4.7
4.9	Optical Images of As-Received Ringhals Weld Overlays Mounted in Epoxy.....	4.7
4.10	Optical Image Providing Overview of the Ringhals Alloy 52 Weld Overlay Sample VY3 After Light Etching and Identifying Various Regions Where TEM Samples were Prepared.....	4.8
4.11	SEM and EDS Compositional Map for Fe Illustrating Location of Hot Cracks in the Dilution Layer Between Alloy 52 and 304SS for Overlay Sample VY3.....	4.9
4.12	Compositional Variation as Measured by SEM-EDS Along the Length and Across a Weld Crack in the Extensive Dilution Zone of the Alloy 52 Overlay.....	4.10
4.13	SEM and EBSD IPF-X Images Illustrating the Microstructure Across the 304SS Base Metal and Weld Metal Interface Region in Overlay Sample VY4.....	4.11
4.14	Optical and SEM Micrographs Illustrating Region where TEM Sample VY3 Originated in the Original Weld Overlay.....	4.12
4.15	Backscatter SEM Images Showing Weld Cracks in Alloy 52 Overlay Sample VY3 and Identifying Region for ATEM Examinations.....	4.13
4.16	TEM Micrograph and Elemental Maps of an IG Crack in Sample VY3.....	4.13
4.17	Higher Magnification Examination of the Crack-Tip Region Shown in Figure 4.16.....	4.14
4.18	Scanning TEM Micrograph and Elemental Maps of a Grain Boundary Leading a Weld Crack in Sample VY3.....	4.15
4.19	EDS Elemental Maps Illustrating Small TiN ₂ Particles and One Large M ₂₃ C ₆ Carbide Along a Grain Boundary Along the Path of a Hot Crack.....	4.16
4.20	SEM-SE Images Illustrating Dendritic Large Grain Microstructure in the MHI Alloy 152 Weld Metal.....	4.17

4.21	Grain Boundary Showing a Single Large Cr-carbide with Numerous Smaller Nb-Ti Carbides	4.18
4.22	Compositional Maps Taken in STEM Mode Revealed that Both Cr-rich and Nb-rich Carbides are Present on the Boundary Between Two Dendrites	4.18
4.23	Photograph Illustrating the Location of Two CT Specimens that were Machined with the Crack Plane Coincident with the 304SS – Alloy 152 Weld Fusion Line	4.19
4.24	Left Image Shows an Optical Micrograph of the Transition Region with the Hardness Indentation Measurements	4.20
4.25	Compositional Map Taken Over the Alloy 152 – 304SS Interface	4.20
4.26	The Line Profile Across the Transition Region Shows that the Ni Changes from ~8 wt% in the Base Metal to ~50% in the Nearby Weld Region	4.21
5.1	Areal Number Density Versus Crack Length for the Weld Cracks Observed in the Ringhals Alloy 52M Overlay Mockup.....	5.3
5.2	Areal Number Density Versus Crack Length for the Weld Cracks Observed in the Ringhals Alloy 52M Inlay Mockup	5.3
5.3	Weld Crack Areal Number Density Versus Length Observed in the MHI Alloy 52 U-groove Mockup	5.4

Tables

4.1	Approximate Region Compositions Based on EDS Measurements	4.8
-----	---	-----

1.0 Background and Research Scope

Weldments continue to be a primary location of stress-corrosion cracking (SCC) in light-water reactor (LWR) systems. While problems related to heat-affected-zone (HAZ) sensitization and intergranular (IG) SCC of austenitic stainless alloys in boiling-water reactors (BWRs) have been significantly reduced, SCC has now been observed in HAZs of non-sensitized materials and in dissimilar metal welds where Ni-base alloy weld metals are used. IGSCC has been observed in both BWR and pressurized-water reactor (PWR) welds and HAZs with recent examples for PWR pressure vessel penetrations (upper and lower head) producing the most concern. Complicating this issue has been a high susceptibility to cracking during welding of the higher Cr replacement alloys (i.e., Alloy 52 and 152). There is a critical need for an improved understanding of the weld metal metallurgy and defect formation in Ni-base alloy welds to effectively assess long-term performance.

A series of macroscopic to microscopic examinations were performed on available mockup welds made with Alloy 52 or Alloy 152 plus selected overlay and inlay mockups. The intent was to expand our understanding of weld metal structures in simulated LWR service components with a focus on as-welded defects. Microstructural features, defect distributions, defect characteristics, and weld residual strains were examined by optical metallography, scanning electron microscopy, electron backscatter diffraction, and transmission electron microscopy. Industry-supplied mockup welds were characterized including Alloy 52 and 152 weldments, Alloy 52M overlay and inlay welds, and an Alloy 52 overlay. The SCC crack-growth rate (CGR) response for many of these materials is being evaluated as part of U.S. Nuclear Regulatory Commission (NRC) projects JCN N6007 and JCN N6782. An emphasis was placed on documenting defects in the representative Alloy 52, 52M, and 152 weldments. Finally, a literature review was initiated on welding-induced cracking in these Ni-base weld metals.

2.0 Materials

2.1 MHI Alloy 52 and 152 Weld Mockups

The Alloy 52 and 152 weld mockups were fabricated by MHI for the Kewaunee reactor and were obtained for primary water stress corrosion cracking (PWSCC) crack-growth testing under NRC project JCN N6007. The mockups were U-groove welds joining two plates of 304 stainless steel (SS) as shown in Figure 2.1. Alloy 152 butter (heat 307380) was placed on the U-groove surface of both mockups by shielded metal arc welding (SMAW). For the Alloy 152 weld mockup, Alloy 152 heat 307380 was also applied as the filler material using SMAW while for the Alloy 52 weld mockup, the Alloy 52 fill (heat NX2686JK) was applied using gas tungsten arc welding (GTAW). Welding parameters for the fill materials were substantially different with the Alloy 152 SMAW having a deposition speed of 4–25 cm/min with a current of 95–145 A and the Alloy 52 GTAW having a deposition speed of 4–10 cm/min with a current of 150–300 A.

One prominent feature in these mockup welds is the presence of a crack starting at the 304SS butt joint at the bottom of the U-groove and extending up into the weld. It appears that the 304SS plate on either side of the butt joint acted as an anchor for the weld, resulting in a stress riser across the slit that drove crack formation and extension into the fill weld. As will be shown in the next section, the extent of the cracking around this stress riser was much greater in the MHI 52 weld mockup.

A relatively long piece of the MHI Alloy 152 mockup was obtained from the Electric Power Research Institute (EPRI) NDE Center, which provided sufficient material to take three slices, X, B, and F, from the mockup for weld crack characterization as described in Figure 2.2. Only a small length of the MHI Alloy 52 mockup was acquired from the General Electric Global Research Center limiting weld defect analysis to a single slice (remaining material was needed for crack-growth specimens).

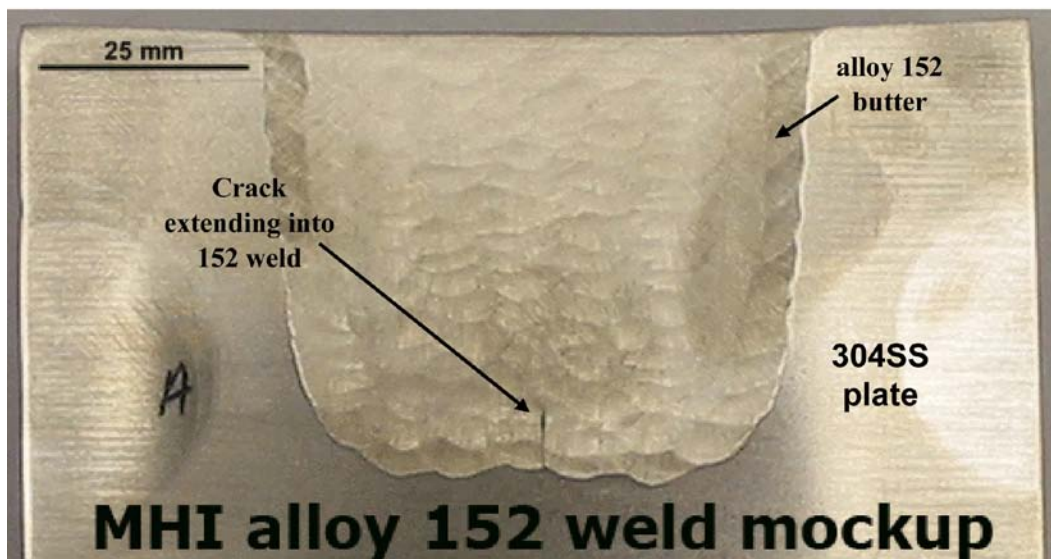
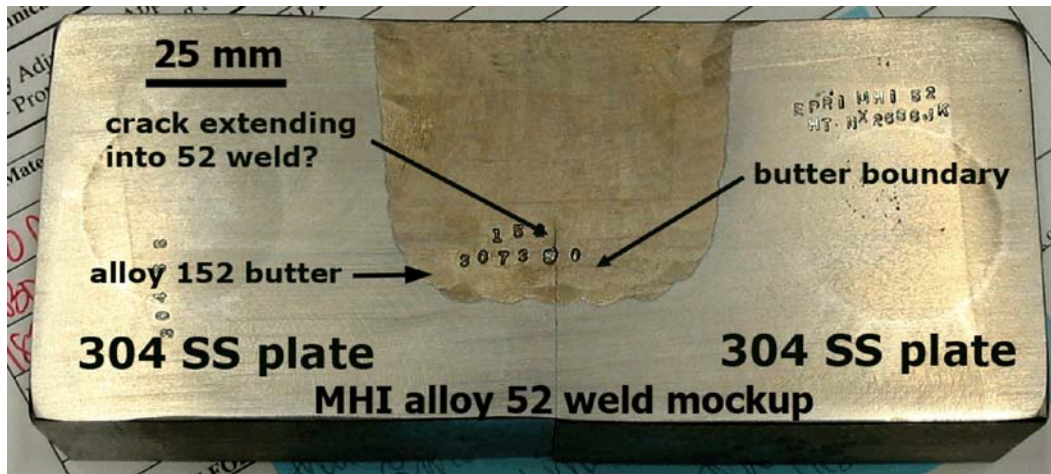


Figure 2.1. Optical Images of MHI Alloy 52 and Alloy 152 Weld Mockups Showing U-groove Weld in Cross Section. Both welds were made to 304SS plate using an Alloy 152 butter layer.

NRC Alloy 152 Weld Test Block
PNNL Slicing Plan 5/06

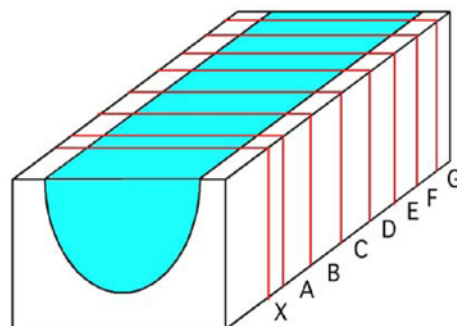


Figure 2.2. Sketch Showing the Relative Location of Slices Taken from the MHI Alloy 152 Mockup

2.2 Ringhals Alloy 52M/182 Overlay and Alloy 52M/82 Inlay Mockups

Two weld mockups made by Ringhals AB were obtained to perform PWSCC crack-growth-rate testing under NRC projects JCN N6007 and N6782. One is described by Ringhals as an overlay mockup, while the other is a full-scale inlay mockup. Crack-growth-rate testing of both materials is in progress with the intent of examining the change in CGR as an SCC crack is grown from the Alloy 182 or 82 weldment into the Alloy 52M weldment. The overlay mockup obtained directly from Ringhals is shown in Figure 2.3. It was fabricated first by robotically welding a 10-mm-thick Alloy 52M layer onto Alloy 690 plate and then by manually welding Alloy 182 onto the Alloy 52M layer. The Alloy 52M layer was applied by GTAW with a weld speed of 7.5 cm/min at a current of 130A while the Alloy 182 was applied by SMAW with a weld speed of 7–12 cm/min at a current of 95–125 A.

The Ringhals inlay mockup piece, obtained from Westinghouse, is from a full-scale inlay repair demonstration on a ring of A533 steel pipe. A boat was carved out of the inner surface of the ring, and as shown in Figure 2.4, Alloy 82 fill was robotically welded onto the pipe section. This was followed by the robotic application of the Alloy 52M inlay. Westinghouse then manually applied an Alloy 152 top layer to allow fabrication of 1T CT specimens with the crack plane lying in the Alloy 82 and growing into the 52M. Details on the welding procedure of the mockup have not yet been obtained; however, both Alloy 82 and Alloy 52M when robotically welded are applied by GTAW. Alloy 152 is typically applied by SMAW.

Two slices were taken from the Ringhals overlay for weld defect characterization, one near the front of the piece (slice A) shown in Figure 2.3 and one near the back of the piece (slice C). A cut plan for the Ringhals Alloy 52M inlay, shown in Figure 2.5, indicates the positioning of the slices used for the weld defect examinations.

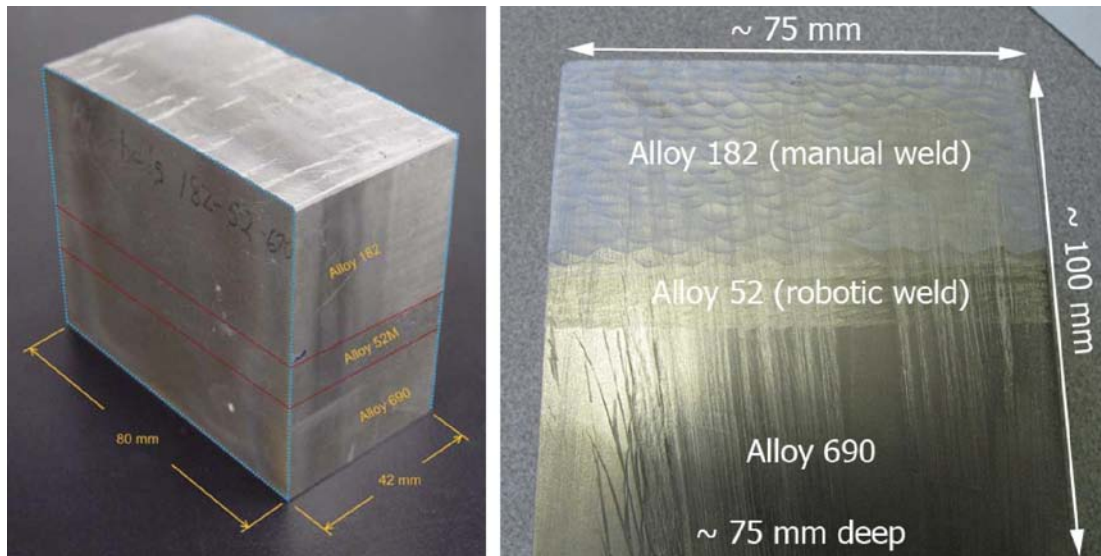


Figure 2.3. Overview of the Ringhals Alloy 52M Overlay Mockup where Alloy 52M was Robotically Welded to an Alloy 690 Plate Followed by Alloy 182 Manually Welded onto the Alloy 52M. The Alloy 52M layer is 10-mm thick.



Figure 2.4. Overview of the Ringhals Alloy 52M Inlay Mockup. This was a full-scale, service mockup with Alloy 82 fill followed by an Alloy 52M inlay. Alloy 152 was welded onto the Alloy 52M by Westinghouse to allow fabrication of CT specimens from the inlay region.

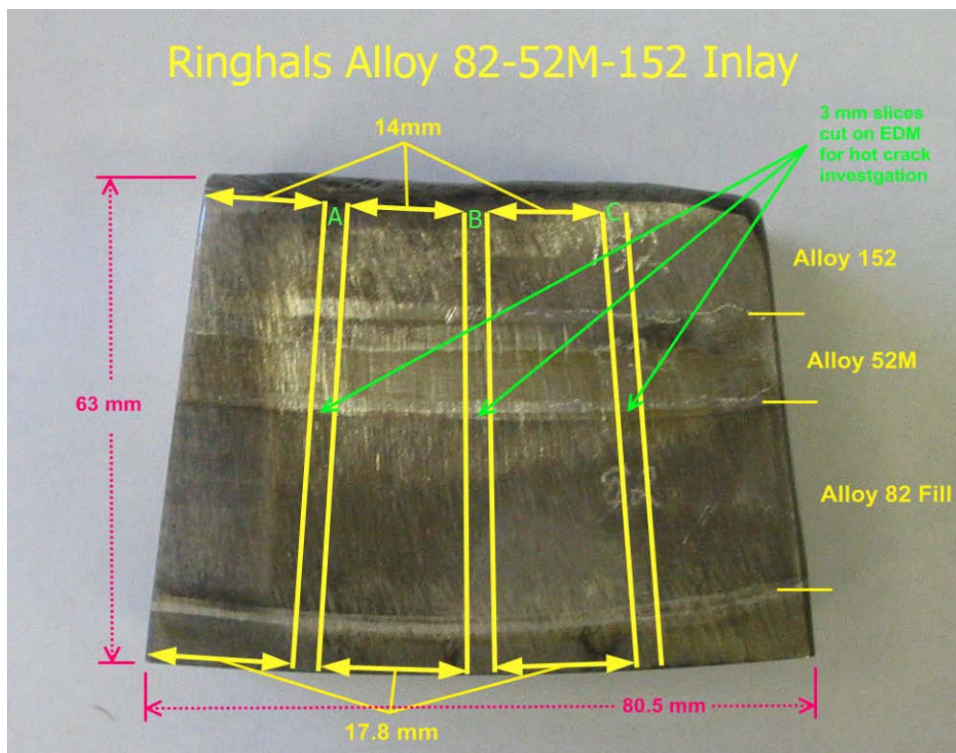


Figure 2.5. Side View of Ringhals Alloy 52M Mockup Showing Cut Lines for CT Specimen Blanks and Metallography Slices

3.0 Metallographic Weld Defect Characterizations

The general approach for all weld defect characterization activities was to polish and etch the available slices from the mockups to reveal the weld and base metal microstructures. Based on the weld structure, a sectioning plan was devised, and the large slices were cut down into a series of smaller pieces that were mounted and polished to a 1- μm finish with colloidal silica. Possible weld defects and cracks were then examined and documented by optical metallography.

3.1 Alloy 152 Weld Mockup

Three slices of the MHI Alloy 152 material were examined for weld defects. The first slice (B) is shown in Figure 3.1. For this slice and all the other MHI weld slices, only those pieces with ID codes in white lettering were examined as these were the expected areas of highest weld residual stress. The small green boxes indicate areas that appeared to contain weld defects in our overview examinations. However, detailed metallography determined that few of these features were cracks. Most were small pits probably resulting from inclusion or precipitate pullout during polishing as shown in Figure 3.2. Only a few cracks were found in the lower right region of the Alloy 152 weld (#08402) and typical small cracks are presented in Figure 3.3. The largest crack was found near the 304SS – Alloy 152 interface, possibly in a region of altered composition. The overview of Alloy 152 slice F in Figure 3.4 shows several locations where cracks were thought to be present in the initial examination. As with slice B, detailed metallographic examination revealed that the majority of small indications were only pits created by pullout of second-phase particles during polishing. An example of this damage and a crack are shown in Figure 3.5. Examination of slice X, shown in Figure 3.6, revealed no cracks except the crack that extended from the butt joint at the bottom of the U-groove weld.

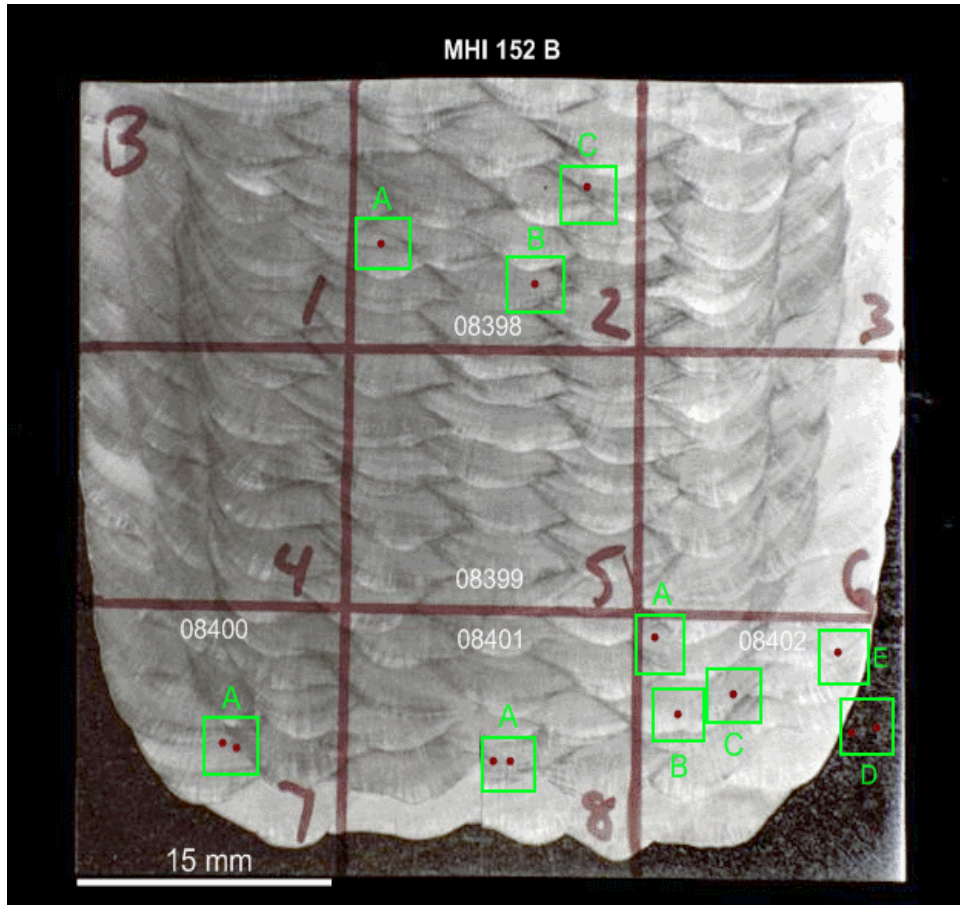


Figure 3.1. Overview Image of the Alloy 152 Weld Slice B with areas Showing Possible Weld Defects Highlighted by the Green Boxes

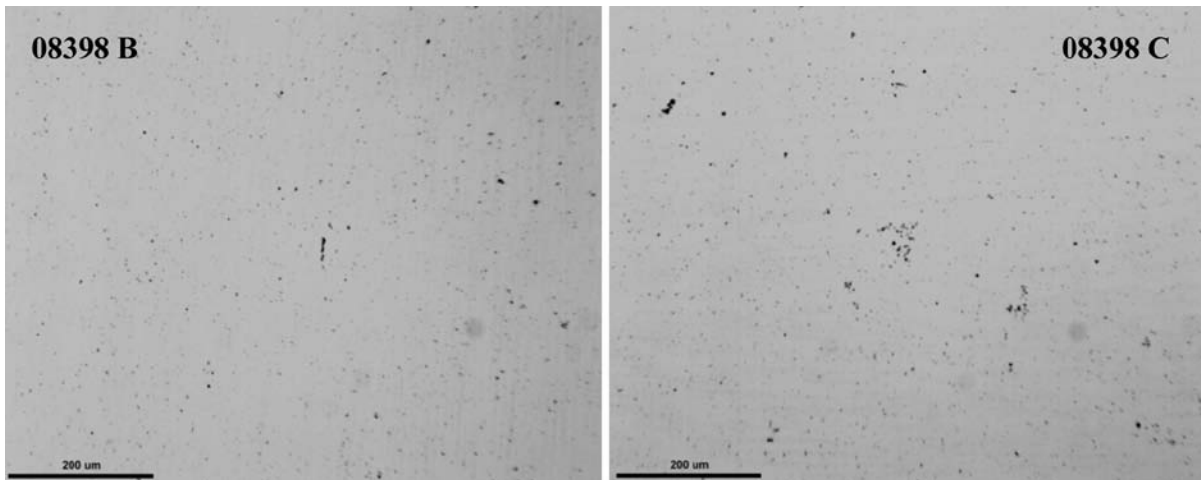


Figure 3.2. Optical Metallographs Illustrating Regions in the Alloy 152 Weld Metal Slice B. Most areas only reveal fine pits due to particle pullout. Scale markers in lower left of each micrograph represent 200 μm .

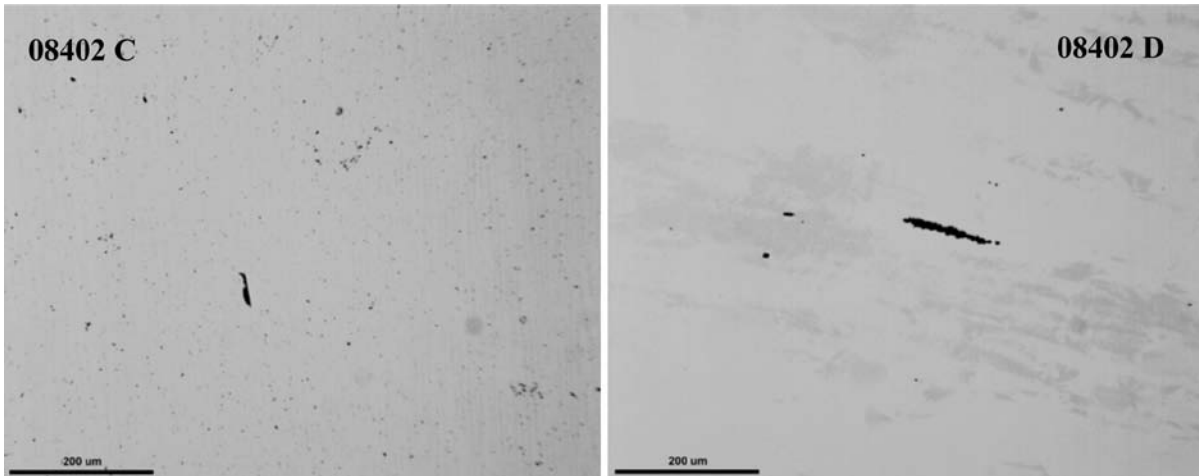


Figure 3.3. Optical Metallographs Illustrating Regions in the Alloy 152 Weld Metal Slice B. The images show small weld cracks, 08402C is in the Alloy 152 weld metal while 08402D is near the 304SS – Alloy 152 interface. Scale markers in lower left of each micrograph represent 200 μm .

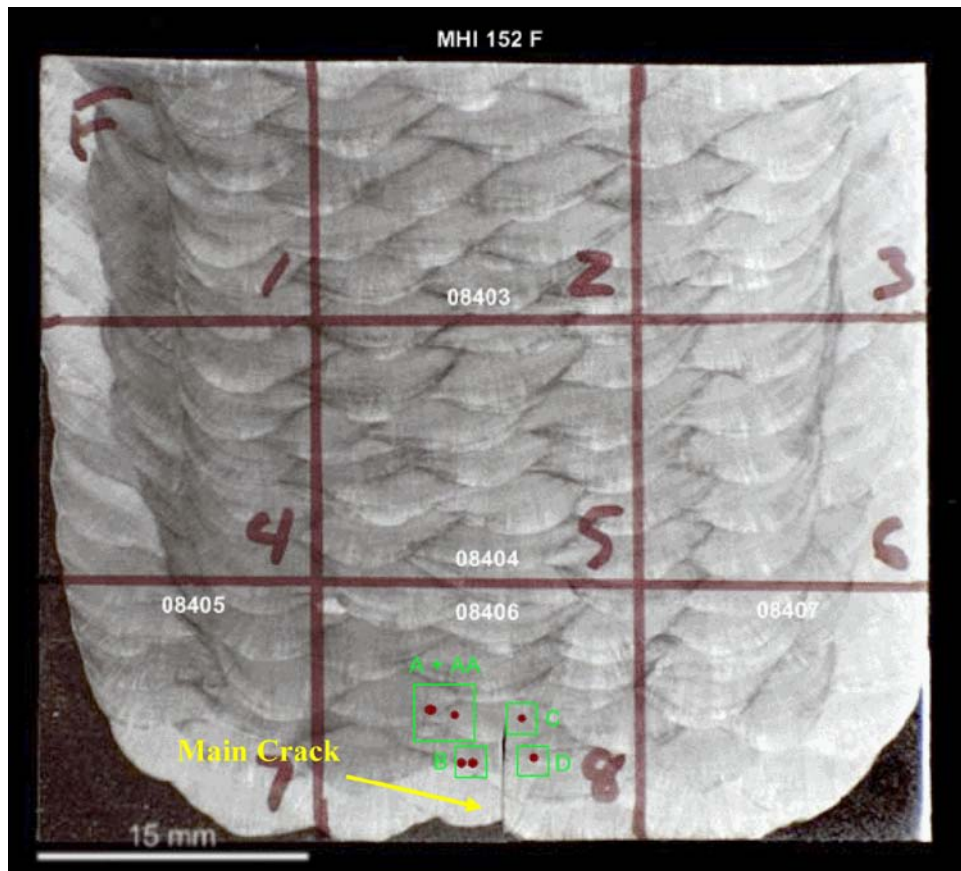


Figure 3.4. Overview Image of the Alloy 152 Weld Slice F with Areas Showing Possible Weld Defects Highlighted by the Green Boxes

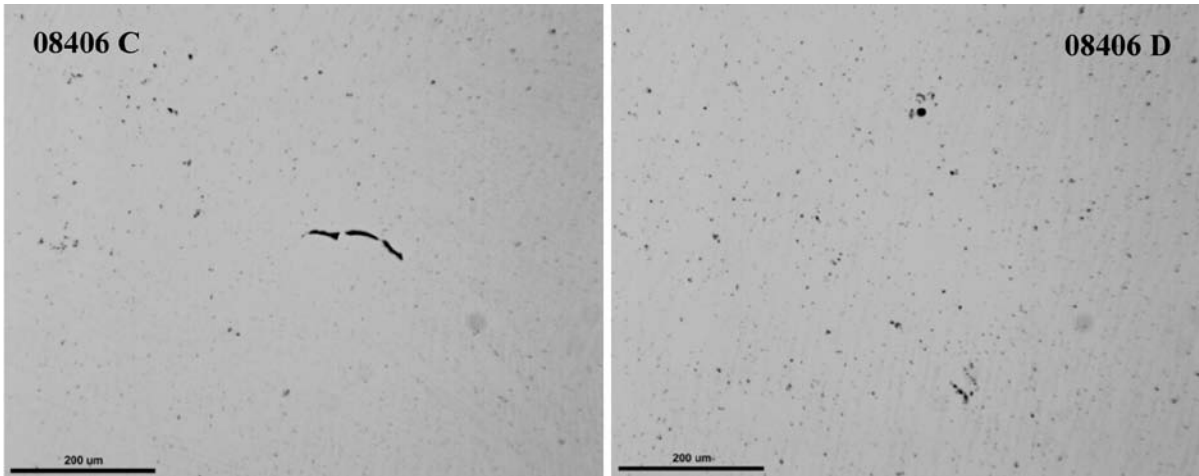


Figure 3.5. Optical Metallographs Illustrating Regions in the Alloy 152 Weld Metal Slice F. Most areas only reveal fine pits due to particle pullout. A small weld crack is seen in 08406C near the main crack. Scale markers in lower left of each micrograph represent 200 μm .

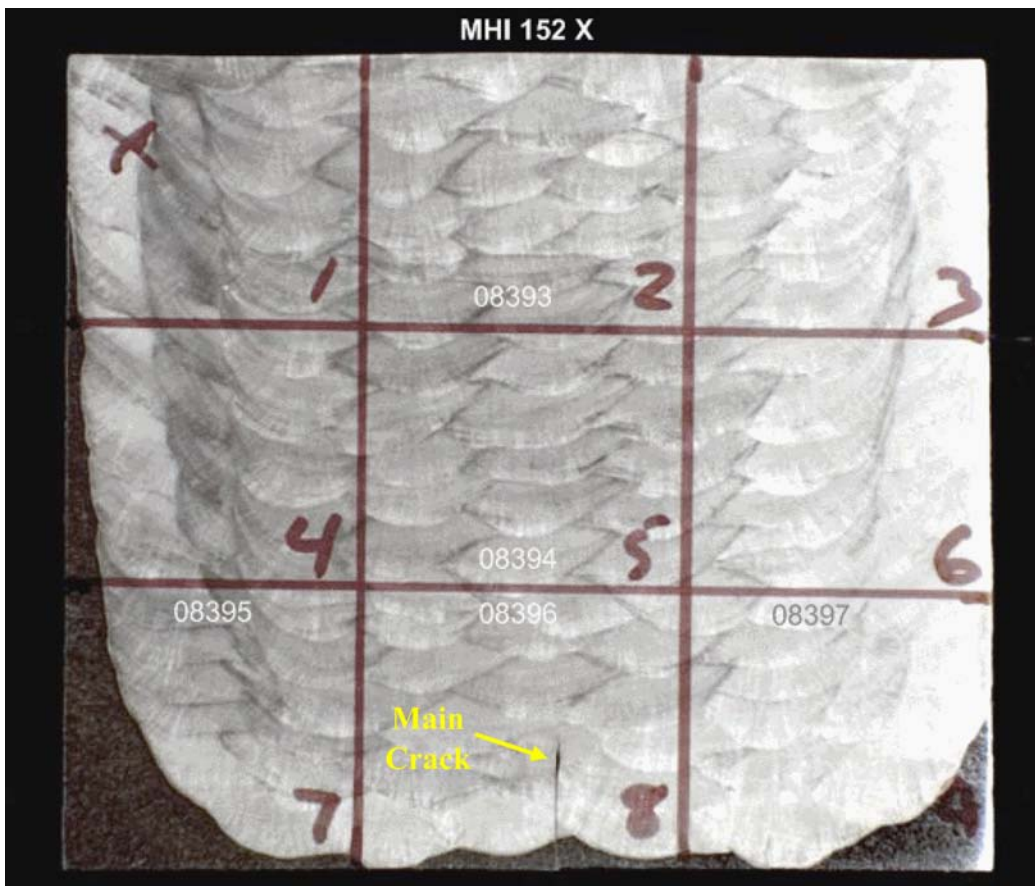


Figure 3.6. Overview Image of the Alloy 152 Weld Slice X. No areas containing weld cracks were identified except for the crack extending from the 304SS joint.

3.2 Alloy 52 Weld Mockup

The Alloy 52 weld, which was fabricated by GTAW instead of SMAW, has a large degree of weld-induced separation at the base of the U-groove where the two plate pieces meet. A long macroscopic crack can be seen extending up through the Alloy 152 butter passes and into the Alloy 52 fill weld as shown in Figure 3.7. Many cracks were identified in the Alloy 52 weld metal around this macroscopic crack with examples shown in Figure 3.8. These cracks are roughly parallel to the large main crack in most instances and span from 300–500 μm in length. Etching of selected cracks, as shown in Figure 3.9, reveals that the cracks are located on grain boundaries as expected. No obvious features can be seen on the cracks that explain their location on these particular grain boundaries. The remainder of the slice was free of any weld defects.

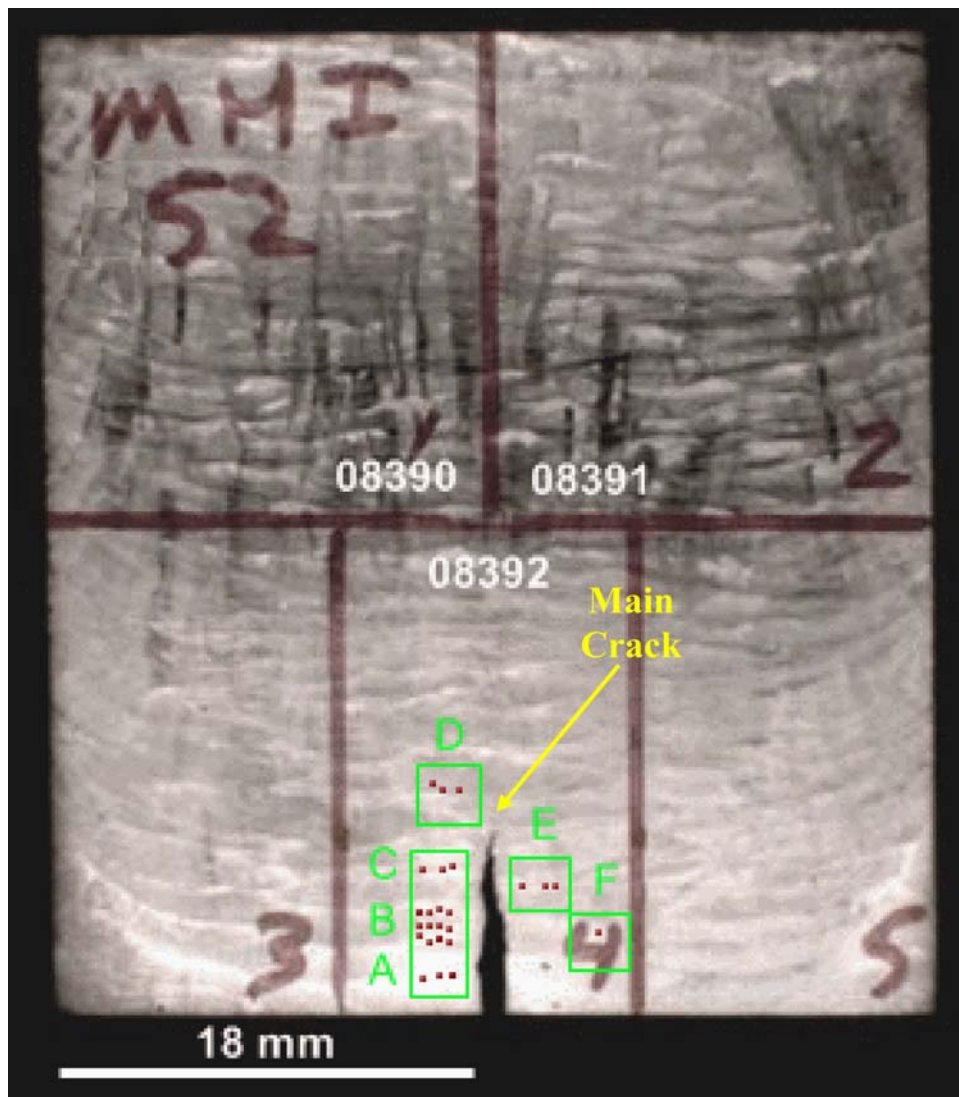


Figure 3.7. Overview Image of the Alloy 52 Slice Showing Large Separation and Cracking Extending Up from the Butt Joint at the Bottom of the U-groove. Large amounts of weld cracks were found in the region around this large crack but nowhere else in the slice.

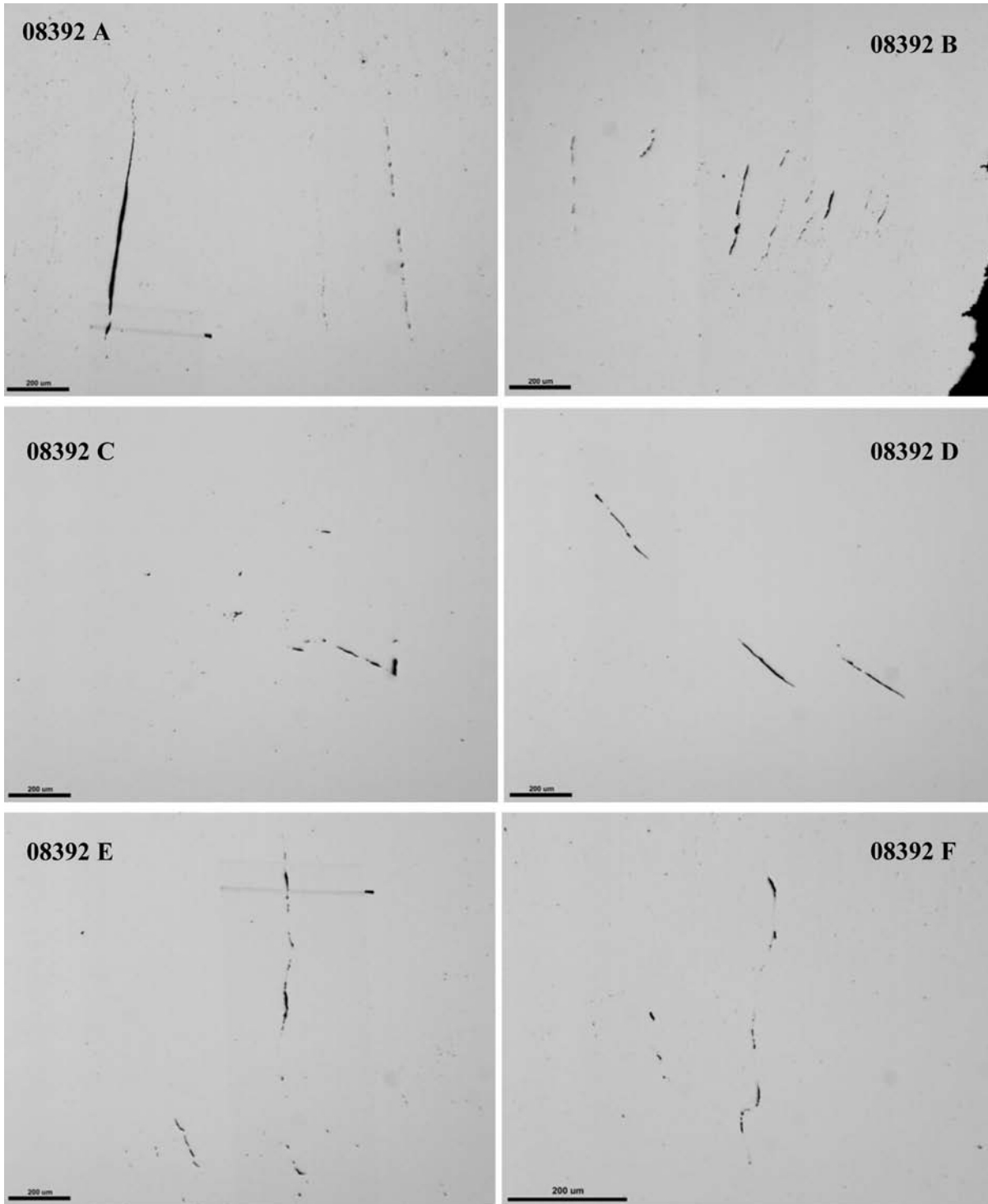


Figure 3.8. Weld Cracks in Alloy 52 Weld Metal Adjacent to Main Crack as Illustrated in Figure 3.7. Scale markers in lower left of each micrograph represent 200 μm .

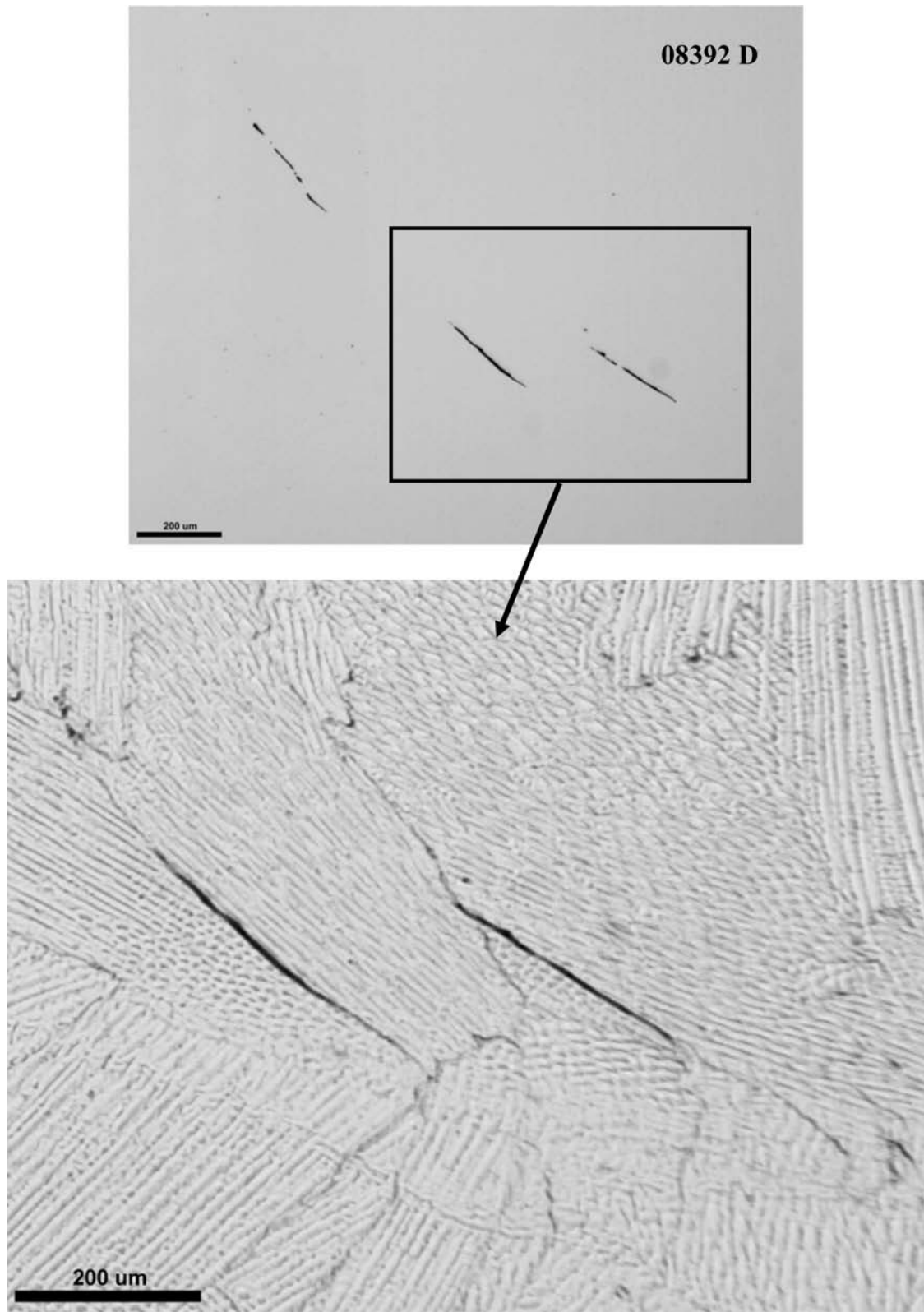


Figure 3.9. Etched Weld Microstructure is Shown to Illustrate the Typical Morphology of the Cracks in the MHI Alloy 52 Weld Metal

3.3 Alloy 52M/182 Overlay Mockup

An overview of the front face slice from the Ringhals Alloy 52M overlay mockup piece is shown in Figure 3.10. Alloy 690 plate is at the bottom of the piece with the Alloy 52M welded onto the 690 and the Alloy 182 welded onto the Alloy 52M. As indicated by the picture, a large number of potential cracks were initially identified. The majority of these were confirmed to be real weld cracks with examples shown in Figure 3.11. The cracks seem to be located in clusters. The cracks in each cluster appear to span the height of the alloy 52M weld with no preference to be located near either the 690/52M interface or the 52M/182 interface. Several weld cracks were also found in the alloy 182 weld as shown in the figure.

Clusters of weld cracks were also found in the back face slice of the Ringhals Alloy 52M overlay mockup as shown in Figure 3.12 with the location of the clusters matching the location found in the front face slice. The clustering of the cracks suggests some characteristic difference in the weld material or welding parameters in these regions on the overlay mockup. Examples of weld cracks found in this back face slice are shown in Figure 3.13. Several of the metallographic specimens were subsequently etched to reveal the location of the weld cracks relative to the grain structure as shown in Figure 3.14 and Figure 3.15. As with the MHI Alloy 52 U-groove mockup, the weld cracks are located on grain boundaries with no outstanding features explaining their presence on these particular interfaces.

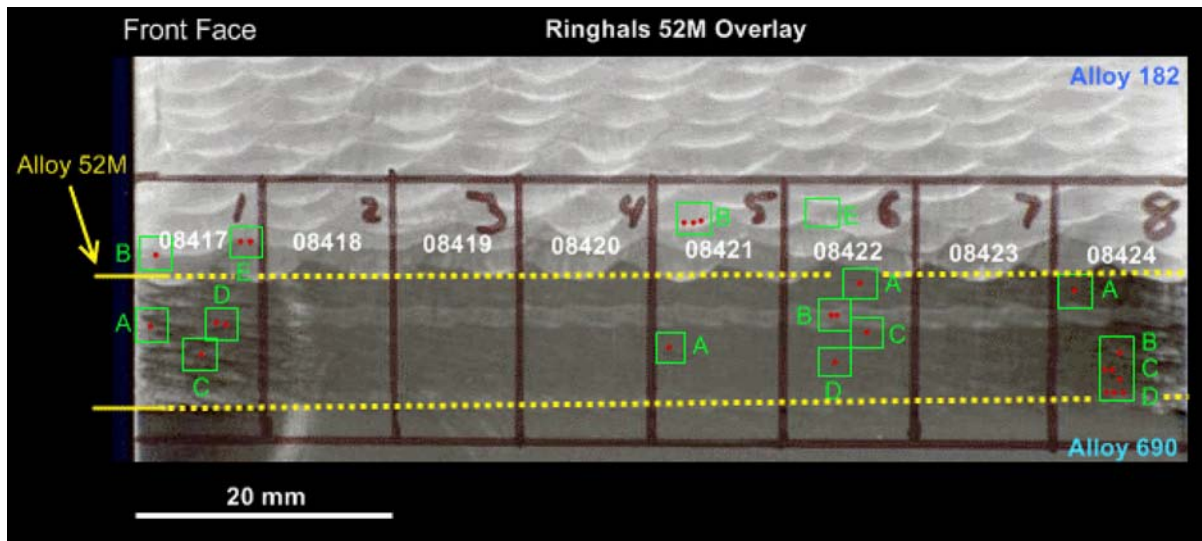


Figure 3.10. Overview Image of the Alloy 52M – Alloy 182 Overlay Slice A (front face) Showing the Alloy 690, Alloy 52M, and Alloy 182 Layers Along with Selected Regions of Analysis

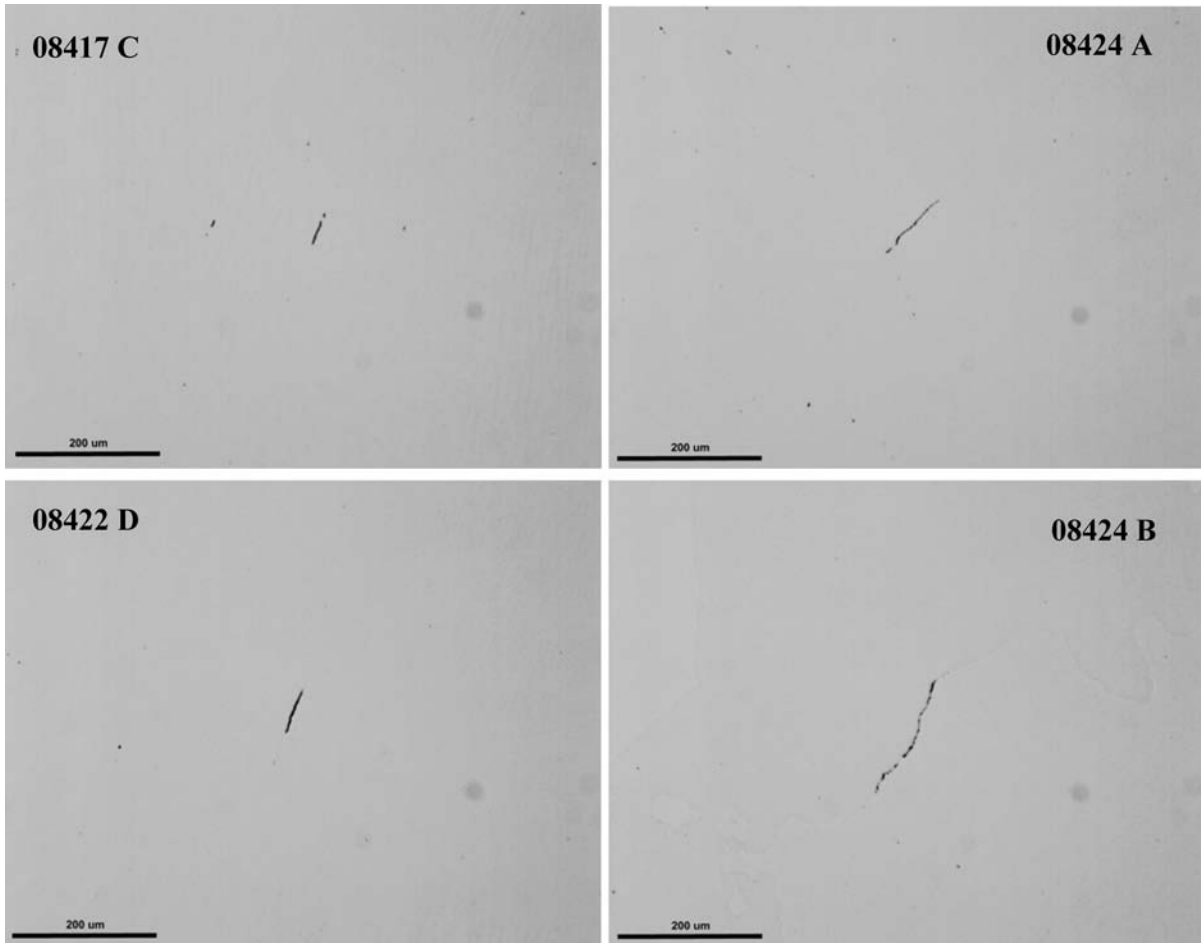


Figure 3.11. Optical Metallographs Illustrating Regions in the Alloy 52M Overlay Slice A (front face) Containing Weld Cracks. Scale markers in lower left of each micrograph represent 200 μm.

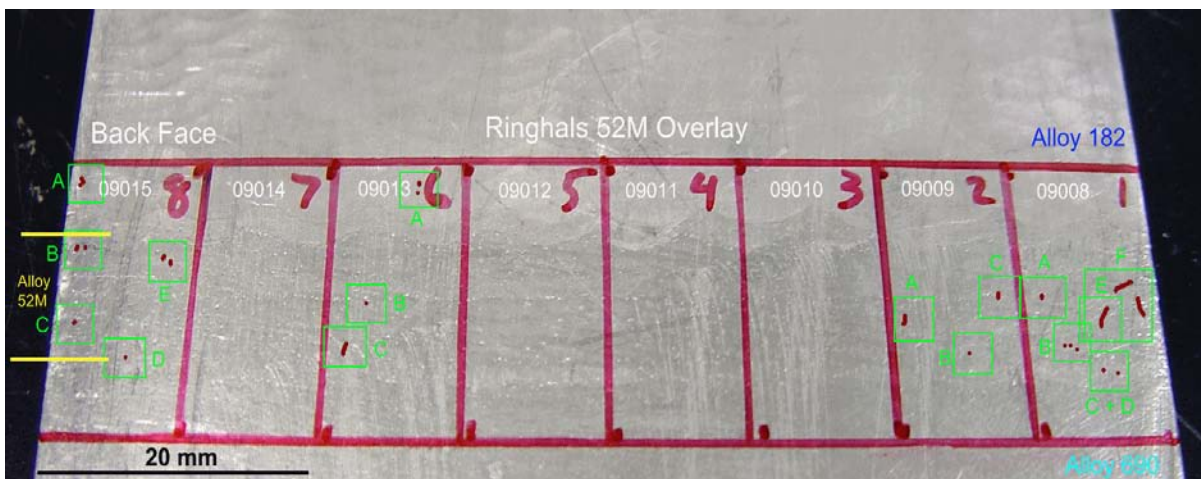


Figure 3.12. Overview Image of the Alloy 52M – Alloy 182 Overlay Slice B (back face) Showing Selected Regions of Analysis

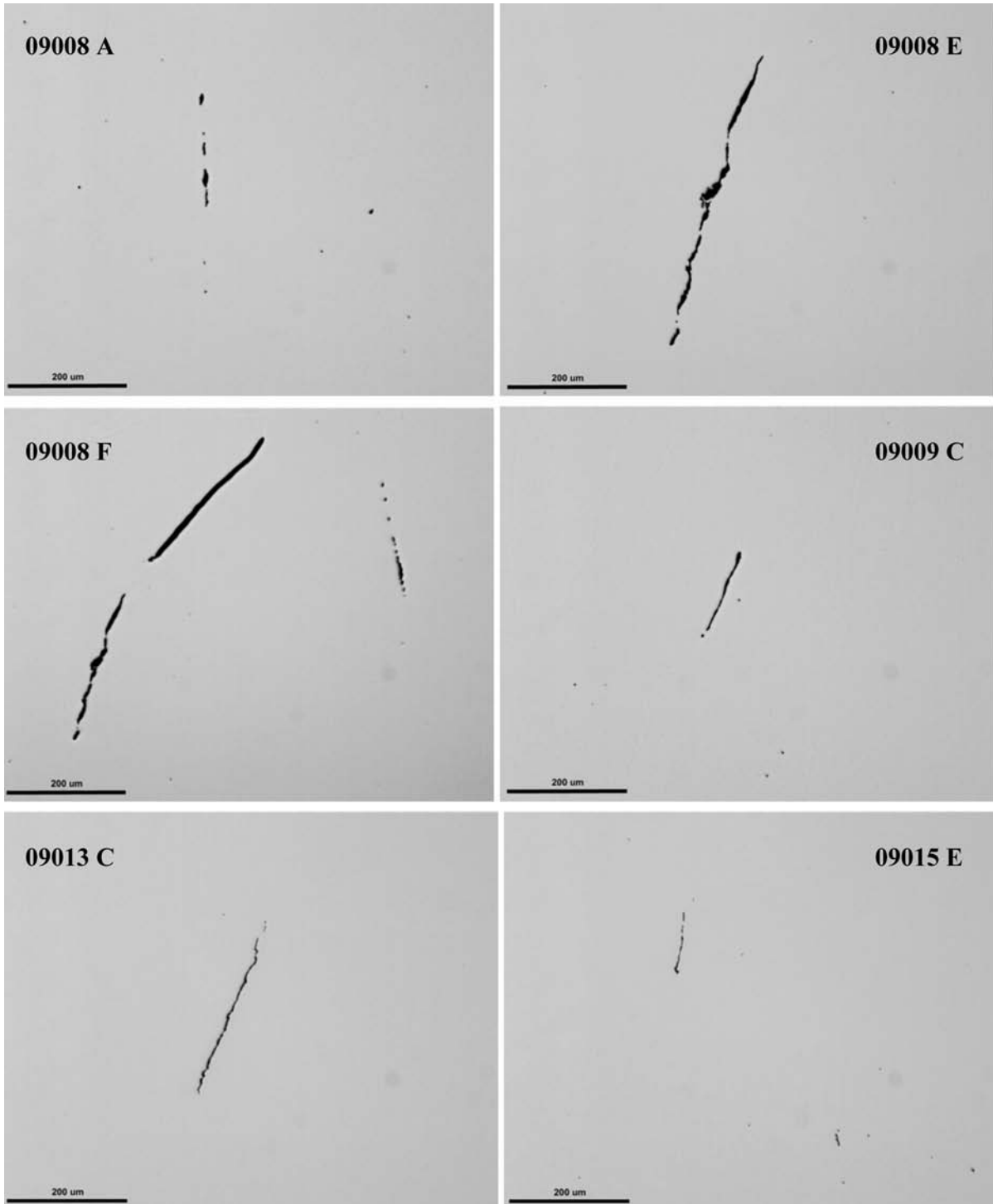


Figure 3.13. Optical Metallographs Illustrating Regions in the Alloy 52M Overlay Slice B (back face) Containing Weld Cracks. Scale markers in lower left of each micrograph represent 200 μm .

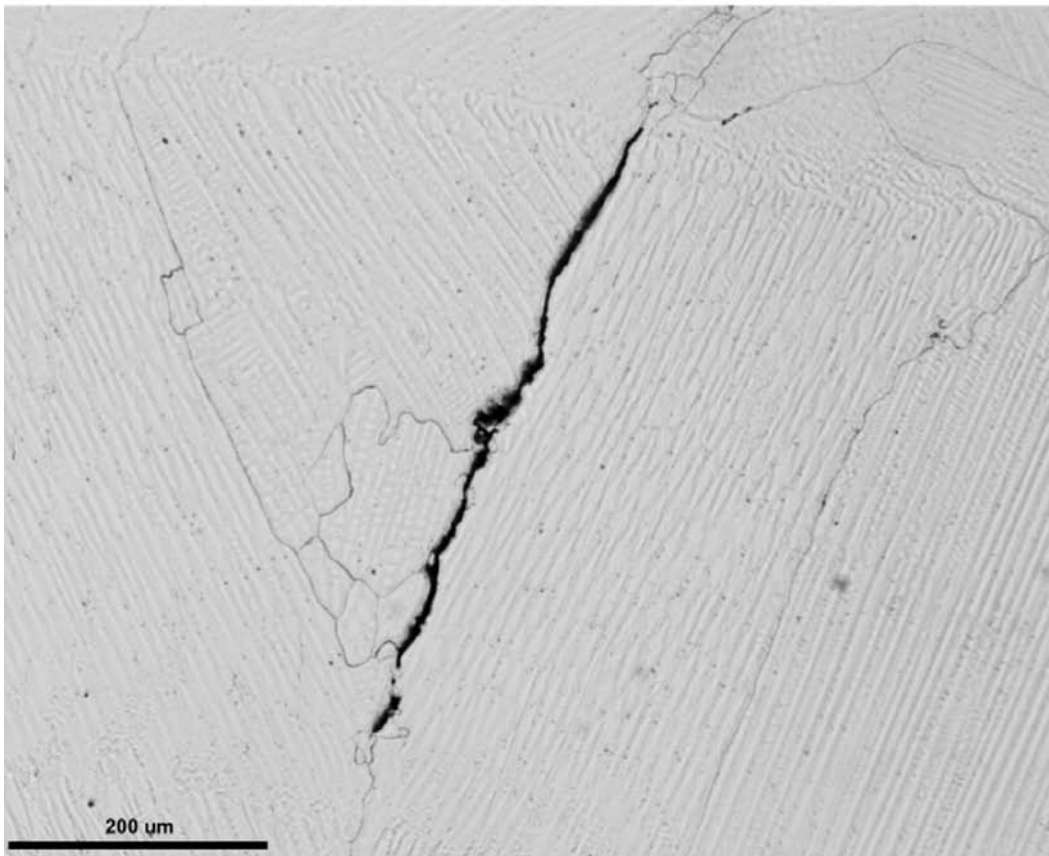
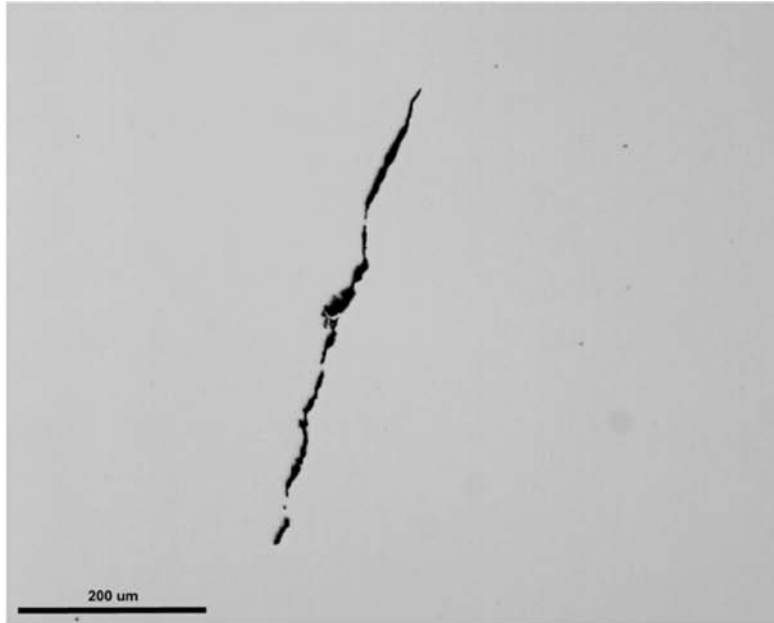


Figure 3.14. Etched Weld Microstructure is Shown to Illustrate the Typical Morphology of the Cracks in the Alloy 52M Overlay

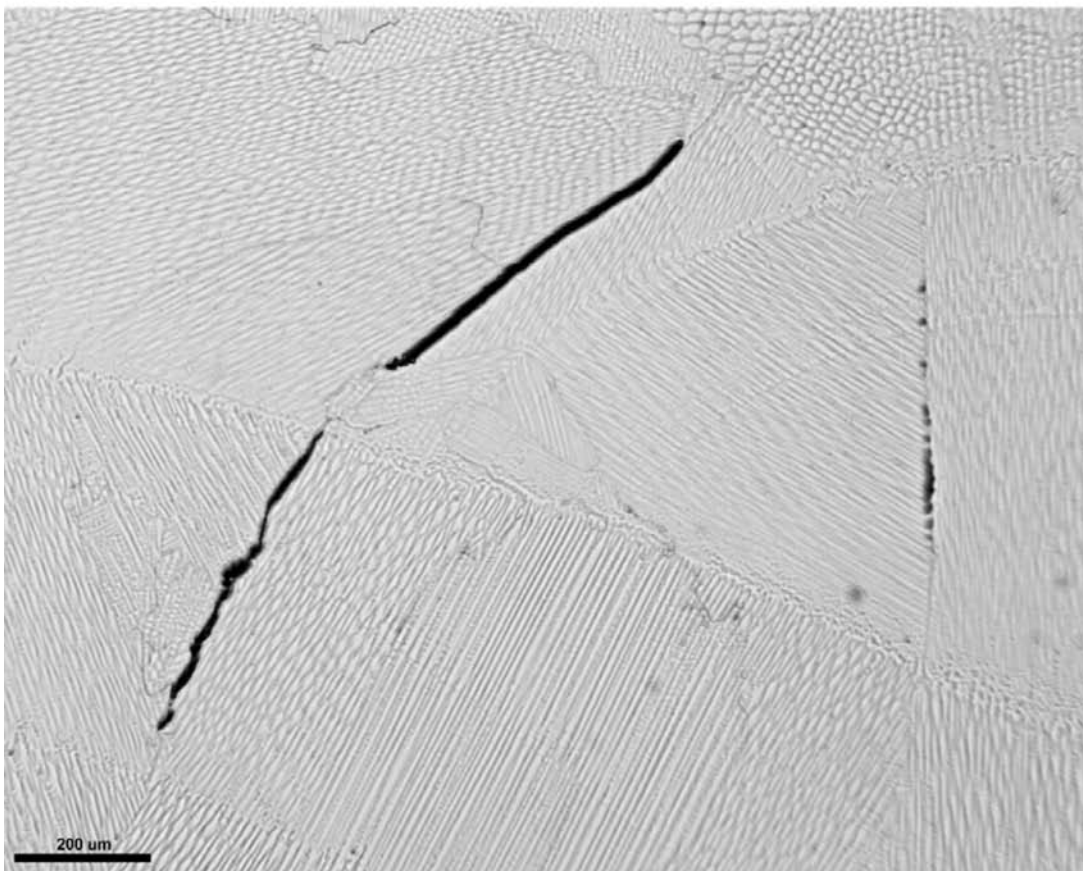
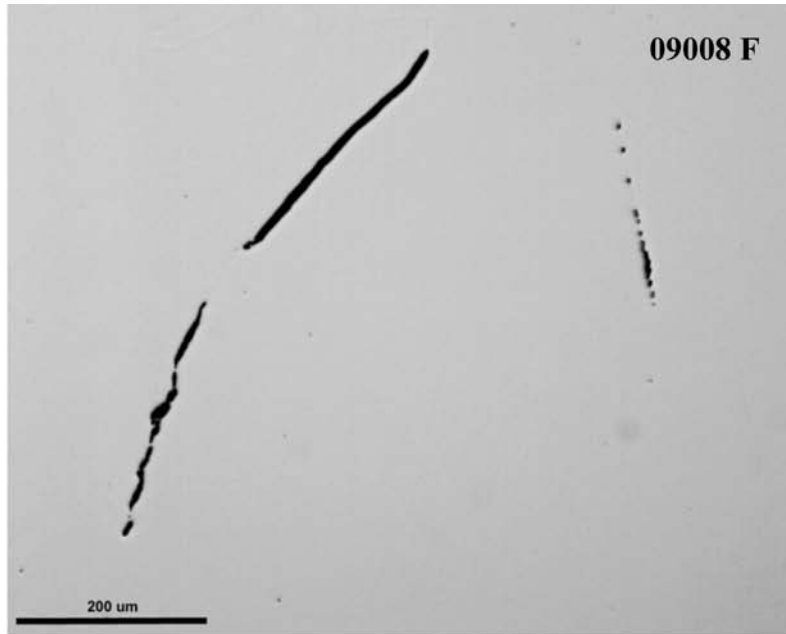


Figure 3.15. Etched Weld Microstructure is Shown to Illustrate the Typical Morphology of the Cracks in the Alloy 52M Overlay

3.4 Alloy 52M/82 Inlay Mockup

An overview of the Ringhals Alloy 52M inlay slice “A” with the cut plan is shown in Figure 3.16. The small green boxes again identify sections that were examined in detail. Several indications of cracking in the upper region of the Alloy 52M weld were observed during preliminary examination, but only one indication was determined to be a weld crack as shown in Figure 3.17. Some small cracks were also found in the Alloy 82 weld metal in one region.

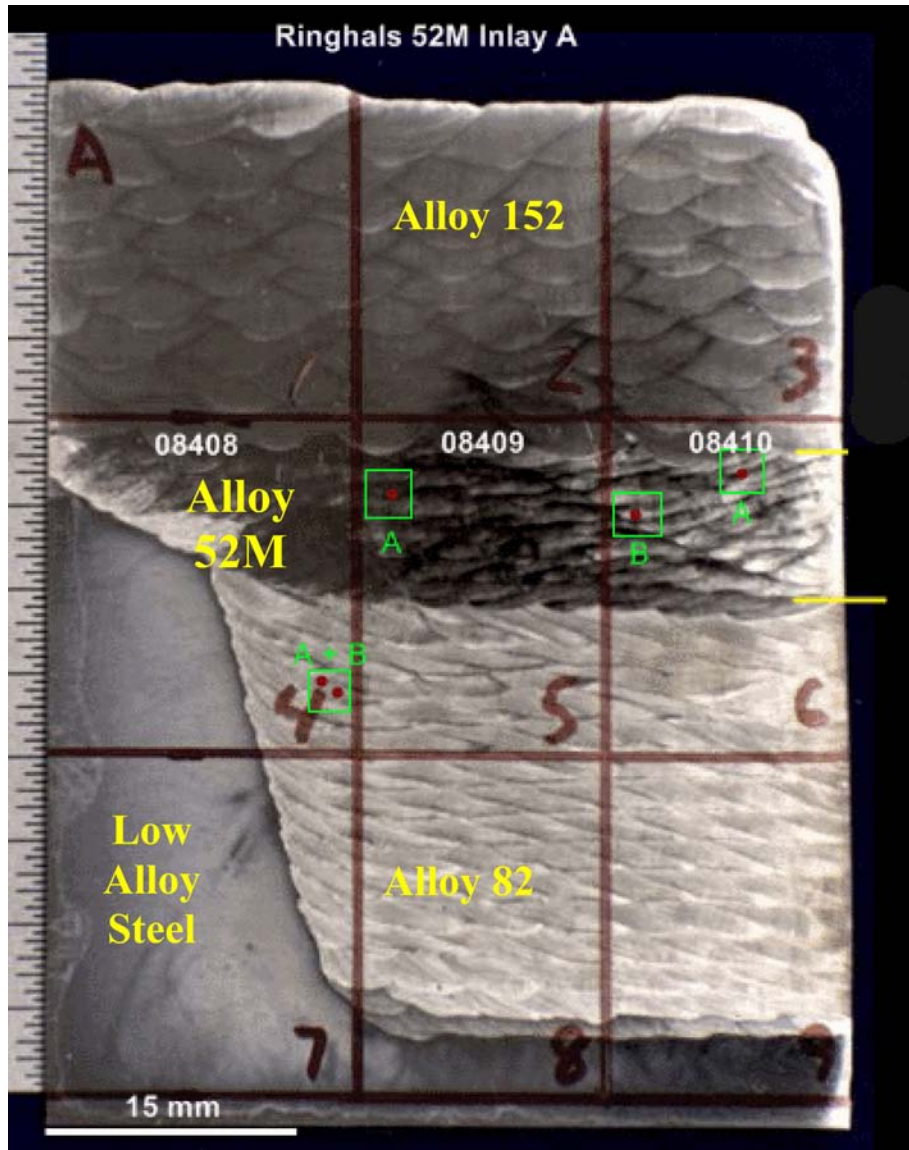


Figure 3.16. Overview Image of the Alloy 52M Inlay Mockup Slice A Showing the Low-Alloy Steel, Alloy 82, Alloy 52M and Alloy 152 Layers Along with Selected Regions of Analysis

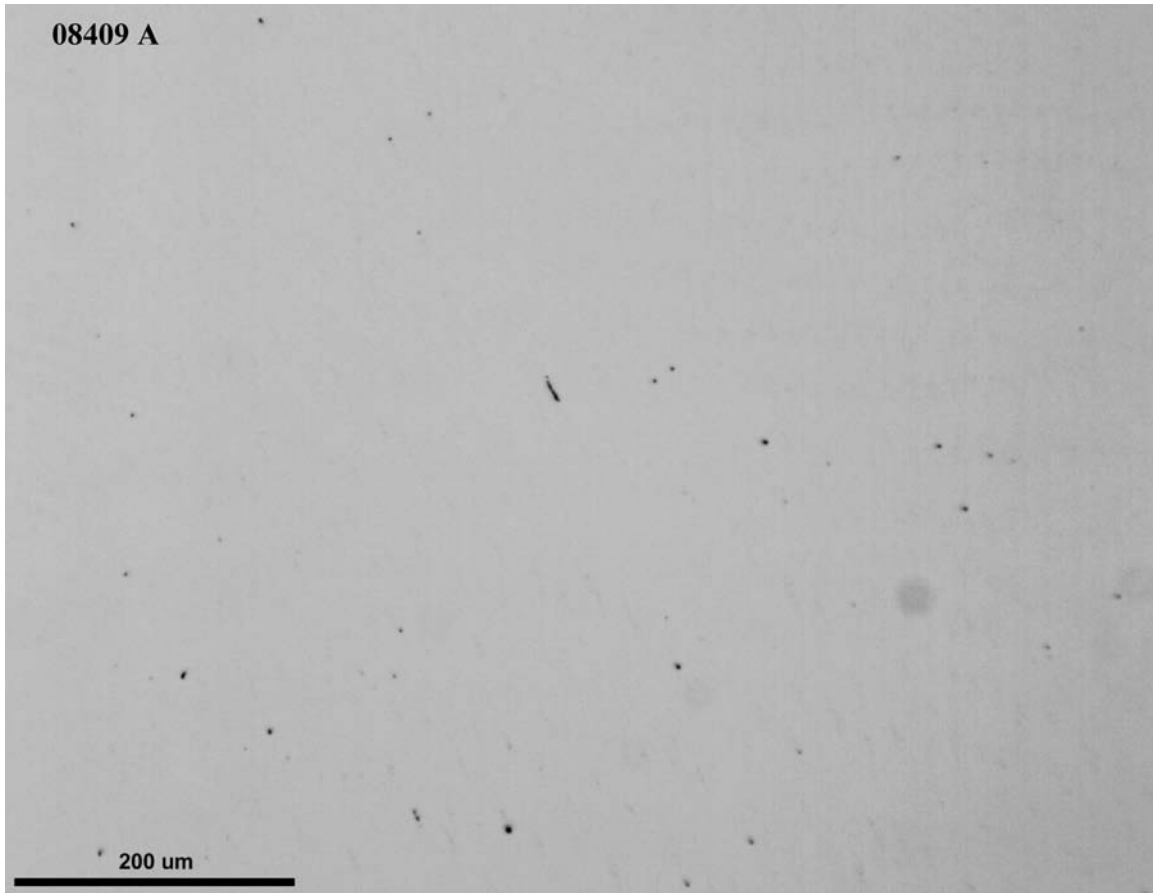


Figure 3.17. Optical Metallograph Illustrating a Region in the Alloy 52M Inlay Slice A Containing Small Pits Probably Resulting from Particle Pullout during Polishing. The only evidence for a weld crack in this slice is shown.

An overview image of the second Ringhals Alloy 52M inlay, slice B, is shown in Figure 3.18. As with slice A, many of the preliminary observations shown in the figure by green boxes were determined to be stringer or inclusion pullout, but overall, there were more confirmed weld cracks in slice B than slice A. The majority of the weld cracks in the Alloy 52M inlay were found to be closer to the Alloy 152 weld interface than the Alloy 82 weld interface. Examples of these cracks are shown in Figure 3.19. Several instances of small weld cracks were also observed in the Alloy 82 repair weld.

An overview image of the Ringhals Alloy 52M inlay mockup, slice C, is shown in Figure 3.20. Several short and long cracks were observed in the Alloy 52M inlay with two examples of longer weld cracks shown in Figure 3.21. The weld cracks were clustered in one region slightly to the right of center of the slice.

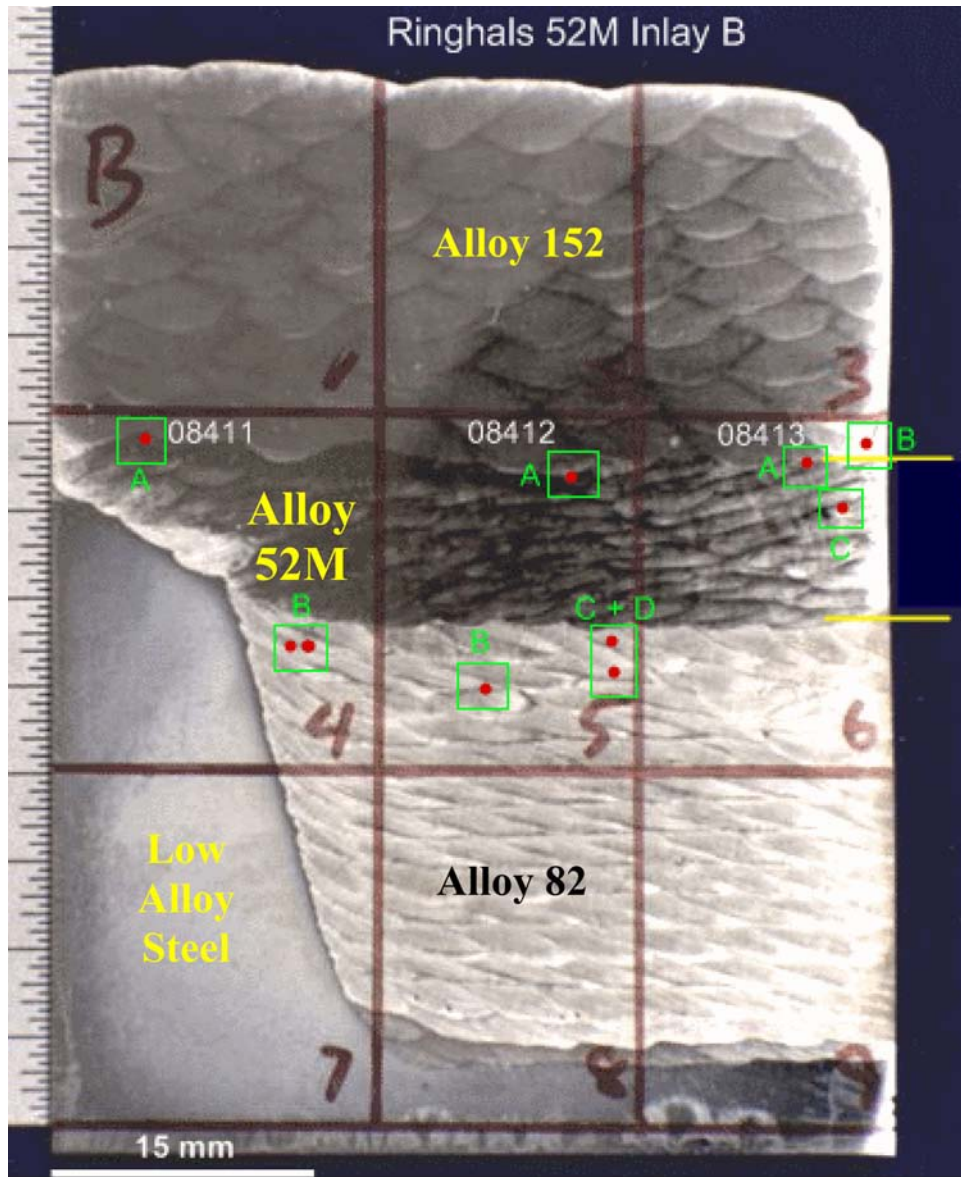


Figure 3.18. Overview Image of the Alloy 52M Inlay Mockup Slice B Showing the Low-Alloy Steel, Alloy 82, Alloy 52M and Alloy 152 Layers Along with Selected Regions of Analysis

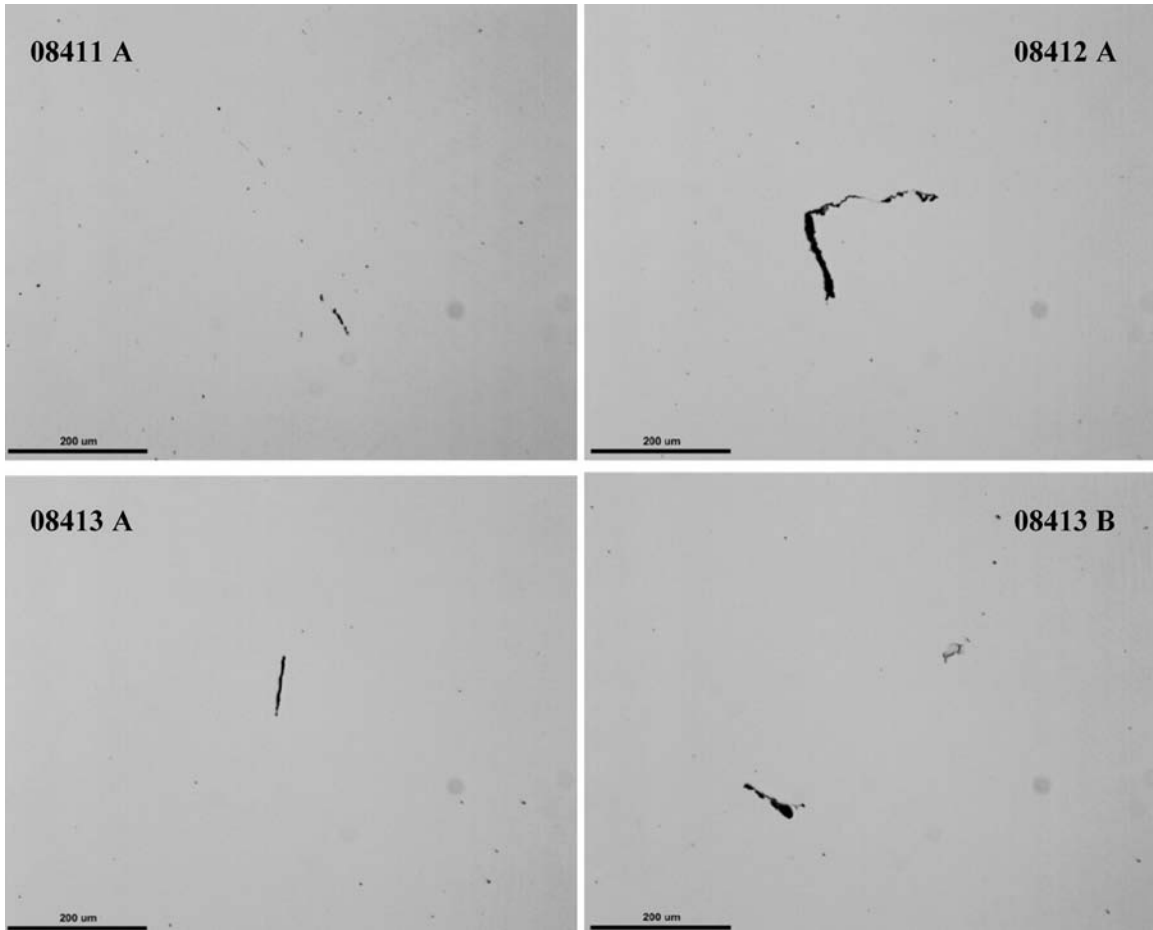


Figure 3.19. Optical Metallographs Illustrating Regions in the Ringhals Alloy 52M inlay Mockup Slice B Containing Small Weld Cracks in the Alloy 52M Weld Metal. Scale markers in lower left of each micrograph represent 200 μm .

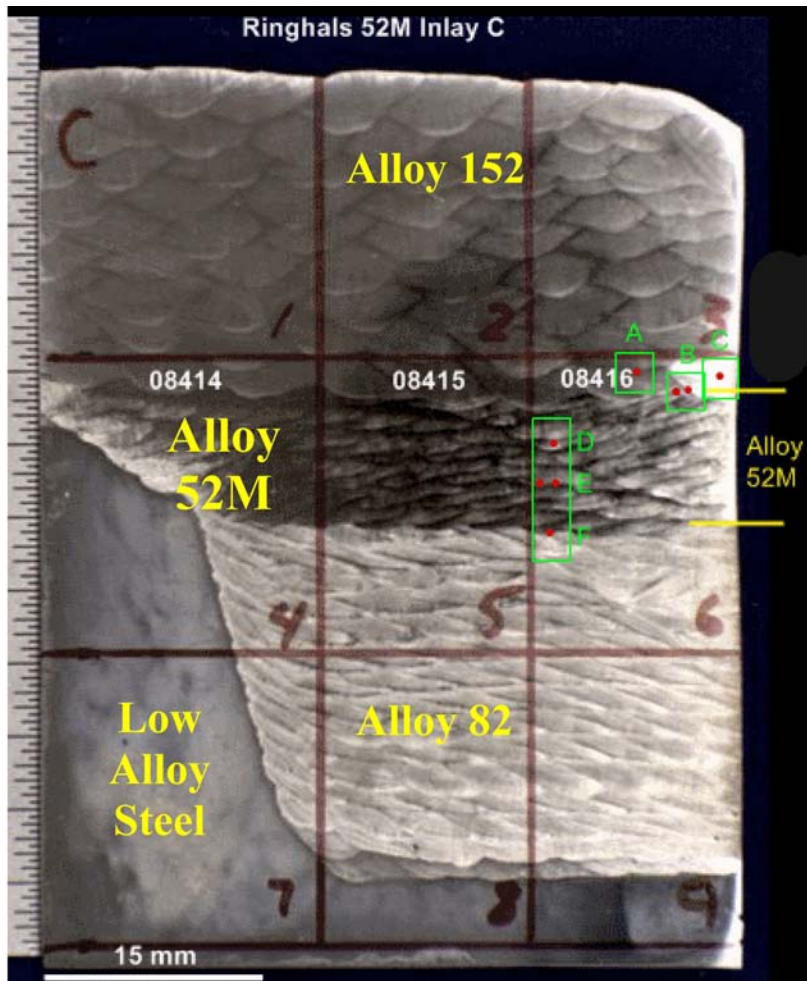


Figure 3.20. Overview Image of the Ringhals Inlay Mockup Slice C Showing Regions Where Indications of Weld Cracks were Observed and Analyzed

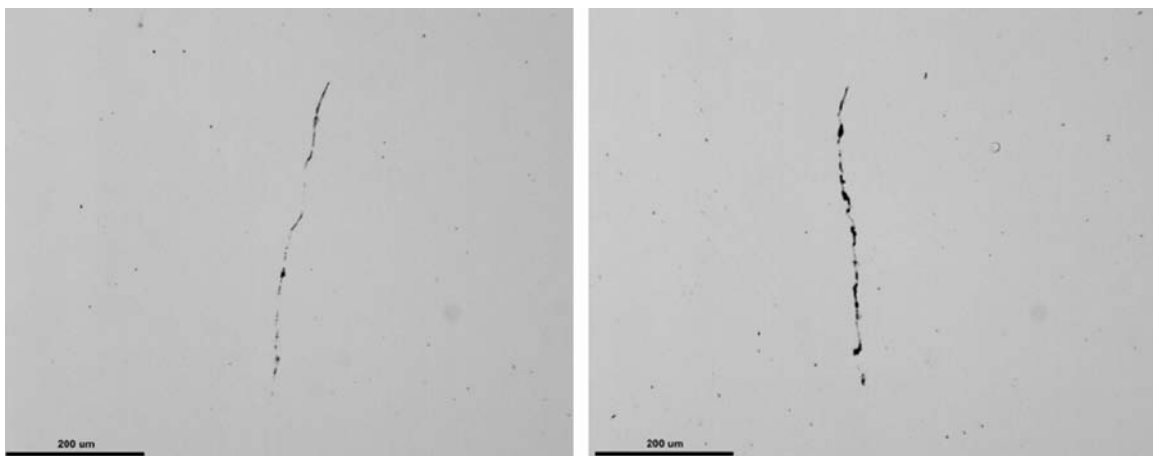


Figure 3.21. Two Examples of Weld Cracks Found in Ringhals Inlay Mockup Slice C. The scale markers on the images represent 200 μm.

4.0 Analytical Electron Microscopy Characterization of Weld Mockups

Selected analytical electron microscopy examinations were performed on the various weld mockups described in the previous chapters. Some of this characterization has been done as part of the current work to generate additional background information on the weld defects detected. Other work was conducted within NRC project JCN N6007 to document weld metal microstructures in regions where SCC crack-growth rates were being evaluated. A more detailed mechanistic assessment of hot cracking in a weld overlay has also been performed under joint sponsorship, initially for Ringhals and then continued under N6007 funding.

Microstructural and weld crack characterization results described here primarily employ scanning electron microscopy (SEM), energy dispersive x-ray spectroscopy (EDS), and electron backscatter diffraction (EBSD) techniques. The Alloy 52M/82 inlay and the Alloy 52 weld mockups were investigated during the current work adding to the optical metallography presented in the previous chapter. These same techniques were used for the mechanistic assessment of hot cracks in an Alloy 52 overlay on a 304SS housing along with high-resolution analytical transmission electron microscopy (ATEM).

4.1 SEM and EBSD of the Ringhals Alloy 52M/82 Inlay Mockup

Just as with the optical metallography results, all the weld cracks that were examined in detail were found to be on grain boundaries. An EBSD pattern quality image and an EBSD inverse pole figure image about the Z axis (IPF-Z) of a Ringhals Alloy 52M inlay specimen (slice C-6) with a short IG crack are shown in Figure 4.1. Color variation in the EBSD IPF-Z image represents variation in crystal orientation with red representing the 001 zone axis pointing out of the image, green representing the 011 zone axis

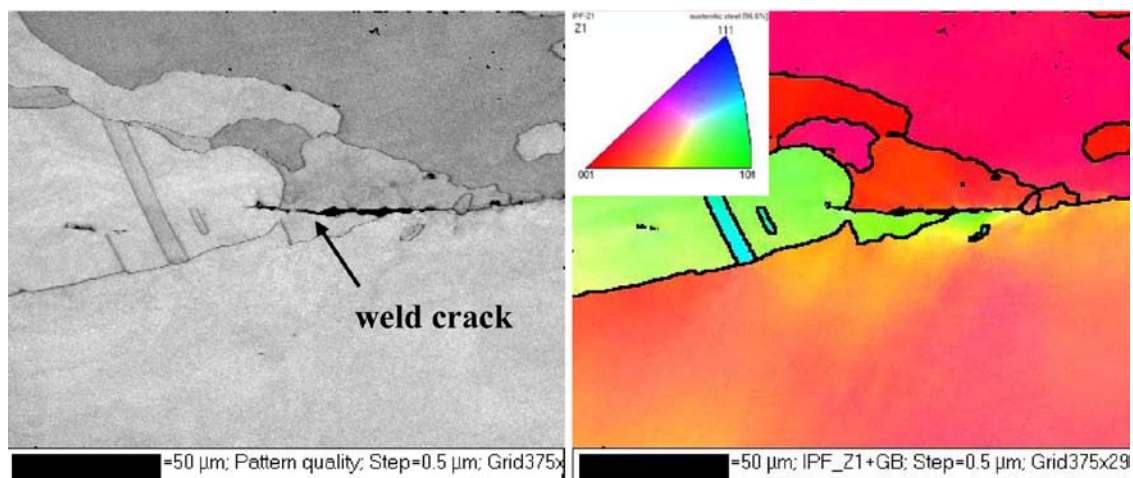


Figure 4.1. EBSD Pattern Quality and IPF-Z Images of a Weld Crack in the Ringhals Alloy 52M Inlay (C-6) Showing Weld Metal Microstructure, Crack Morphology, and Areas of Deformation

pointing out of the image, and blue representing the 111 zone axis pointing out of the image (as shown in the inset legend). The IPF shows several interesting features. The step change in color above and below the crack indicates that the crack lies on a high-angle grain boundary, and it can be seen that the crack appears to have propagated along a straight section of grain boundary and blunted in the adjoining grain matrix as the boundary turned ~90 degrees. Color variation in the grain below the crack indicates a large amount of plastic deformation, especially just below the crack where the color changes from green to yellow and then to red. SEM-EDS maps in Figure 4.2 reveal dendritic solidification segregation (e.g., Nb and Mn) in the grains above and below the crack. This also suggests that this is a high-angle, high-energy

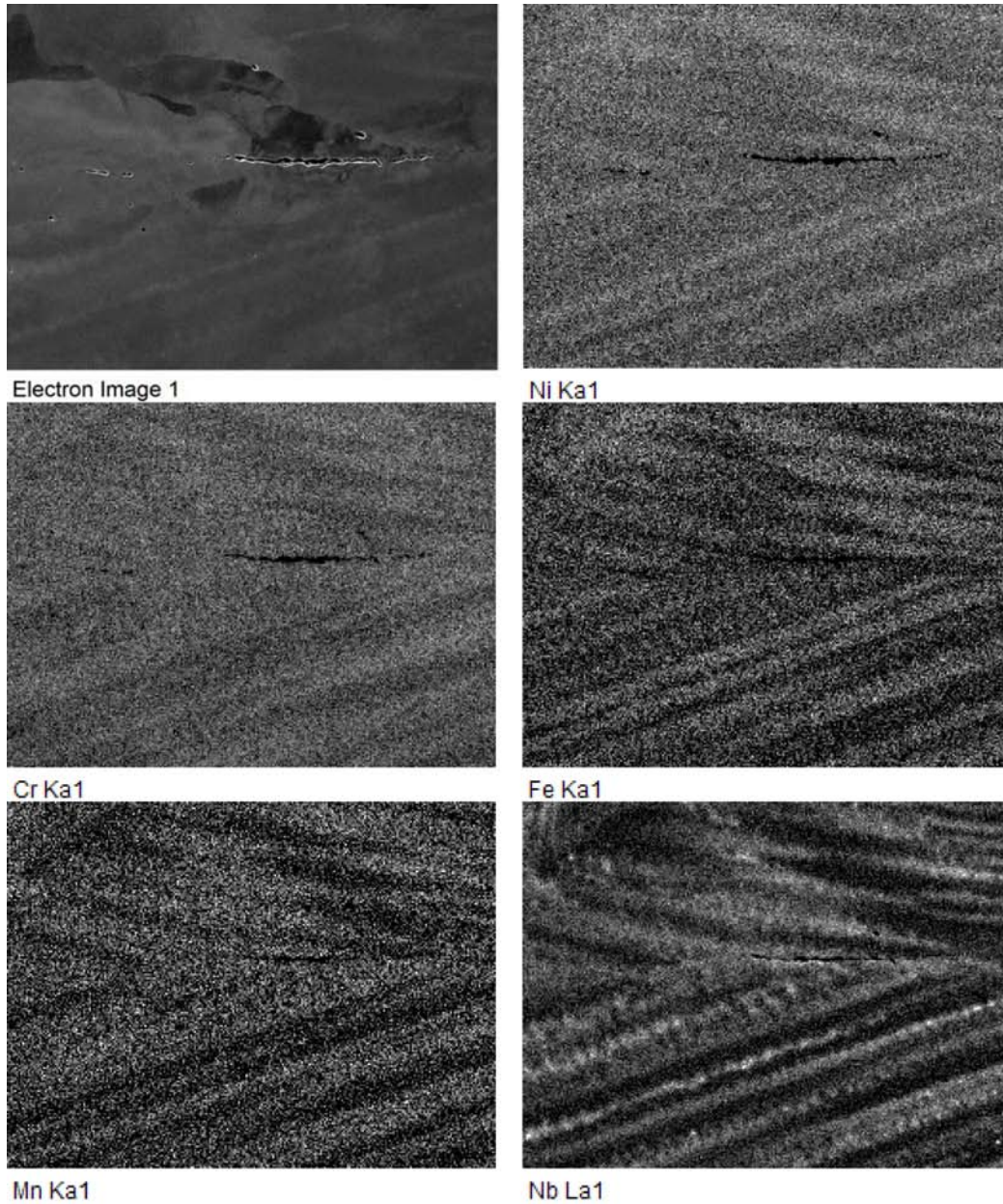


Figure 4.2. SEM-BSE Image and EDS Maps of the Ringhals Alloy 52M Inlay Weld (C-6) Revealing Significant Compositional Variations within Grains Particularly for Nb

boundary and more susceptible to cracking. What is not observed is any strong compositional variation associated with the grain boundary itself. It is important to note that the resolution of SEM-EDS analysis is limited and composition changes of at least micron dimensions must be present to be detected. As a result, fine-scale segregation or precipitation will not be detected. Additional examinations by ATEM are needed to better define the grain boundary characteristics that may be involved in the cracking process. Examples of this approach to investigate crack tips and grain boundaries on the nanoscale are given later in this chapter.

4.2 SEM and EBSD of MHI Alloy 52 U-Groove Weld Mockup

As described in the previous chapter, the MHI Alloy 52 U-groove weld mockup has a high density of cracks adjacent to the center main crack (see Figure 3.7) that extended from the stainless steel fit-up joint. This location suggested that cracking was promoted by high local stresses during solidification of individual passes. An SEM and EBSD examination of the weld cracks and strains was conducted and focused on the three regions shown in Figure 4.3. An extensive distribution of IG cracks can be seen involving a high fraction of grain boundaries along the length of the grains. Each of these regions was

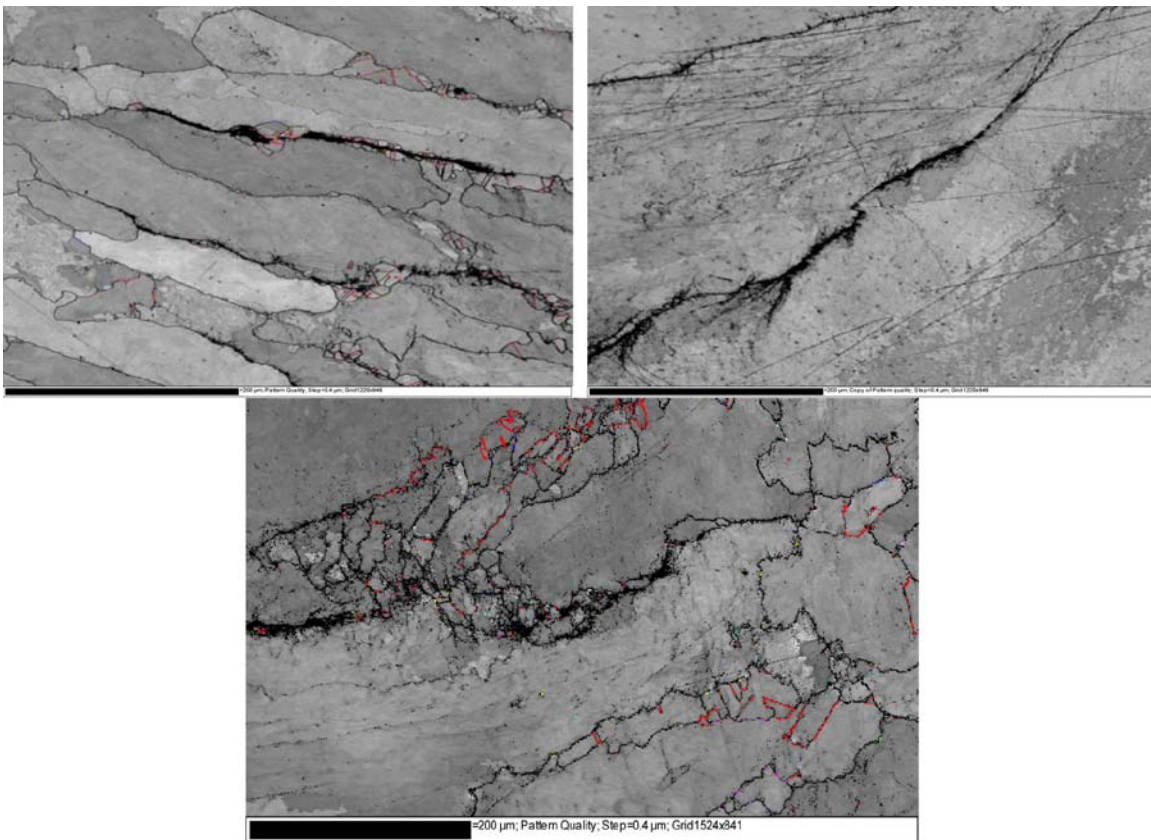


Figure 4.3. EBSD Pattern Quality Images of Three Regions of Cracks in the MHI Alloy 52 U-Groove Weld Where EBSD Characterization was Performed. Each region is near the main center crack shown in Figure 3.7 and these cracks are represented by the optical images in Figure 3.8.

examined in more detail by EBSD techniques and examples are shown in Figure 4.4 through Figure 4.6. The EBSD IPF-Z image in Figure 4.4 enables a better visual image of the individual weld metal grains and highlights areas of plastic deformation. The typical large, elongated grains can be seen plus a collection of very fine grains along certain grain boundaries. The fine grains present along the cracks suggest that local recrystallization may play some role in the cracking process. High strains depicted by large changes in crystal orientation within a grain in Figure 4.4 are found at many of the high-angle grain boundaries and within the interior of many of the grains.

Cracks following two boundaries encompassing a large weld metal grain are presented in Figure 4.5. The EBSD IPF-Z image shows a significant change in orientation near the cracks and within the large grain itself indicating very large strains within this grain. The grains bounding the other side of the cracks, however, have very little indication of strain. The lack of indicated strain in this grain may be a limitation of the IPF-Z image because crystal rotations around the normal axis to the image are not captured by an IPF-Z image.

The final cracked region examined (Figure 4.6) also shows a mixture of large, elongated grains and local regions of very fine, recrystallized grains. A complex distribution of open and tight cracks is present in this region. As expected, high strains indicated by the strong color variations within many of the grains are found associated with cracks and grain boundaries in this entire region.

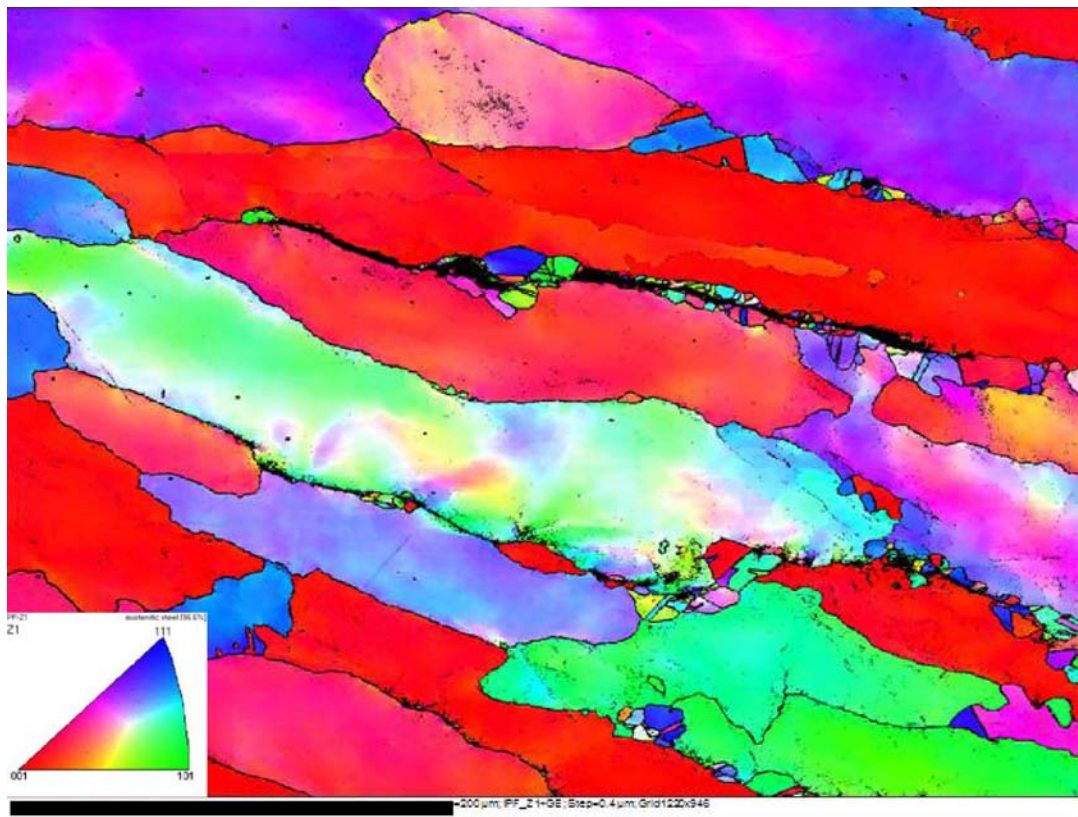


Figure 4.4. EBSD IPF-Z Illustrating the Differences in Grain Orientations and Deformation in the Vicinity of the MHI Alloy 52 U-groove Weld Cracks

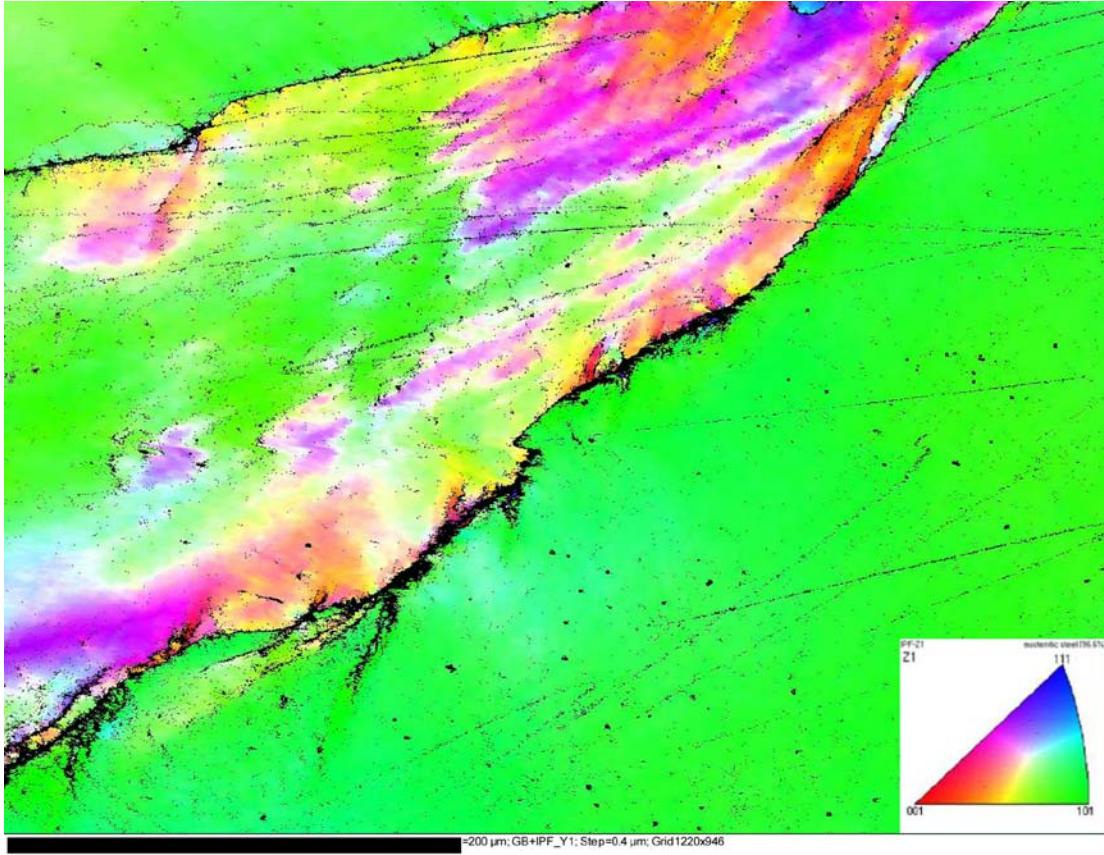


Figure 4.5. EBSD IPF-Y Image Illustrating Differences in Grain Orientation and Rotation Around Weld Cracks that Formed Along High-Energy Grain Boundaries in the MHI Alloy 52 U-groove Weld

Additional general characterizations were performed by SEM and SEM-EDS techniques on the MHI Alloy 52 U-groove weld mockup. Compositional variations in the Alloy 52 weld metal and in the cracked regions were assessed by selected SEM-EDS maps as illustrated in Figure 4.7. Minor indications of Mn and Nb segregation were seen associated with matrix dendrites, but no local enrichment of alloying or impurity elements to grain boundaries could be detected at the resolution level attained with this instrument.

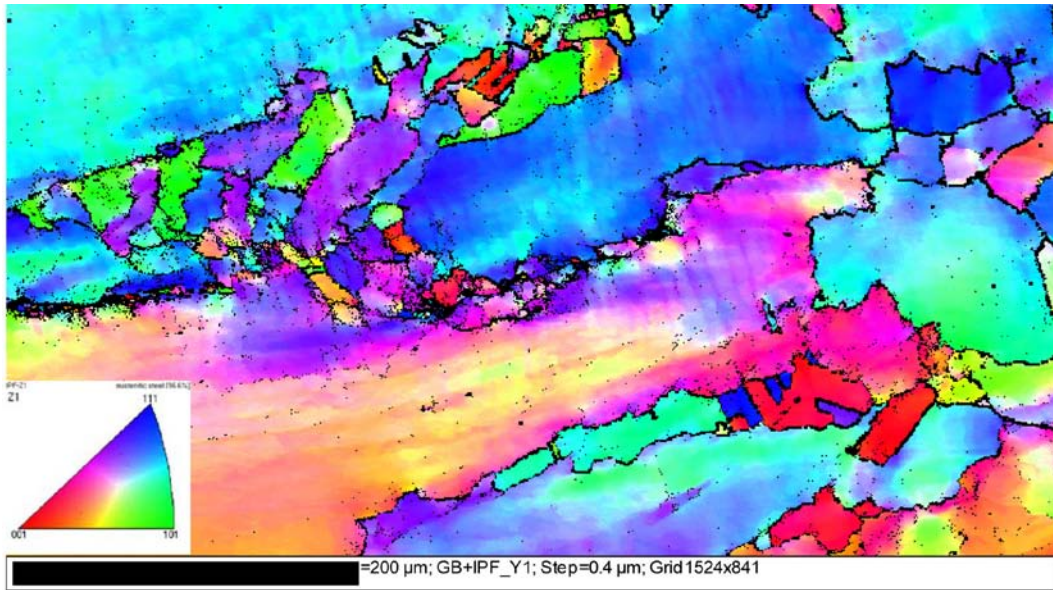


Figure 4.6. EBSD IPF-Y Image of the MHI Alloy 52 U-groove Weld Illustrating Differences in Grain Orientation and Deformation Near Weld Cracks Situated Along High-Energy Grain Boundaries and Regions of Fine Grains

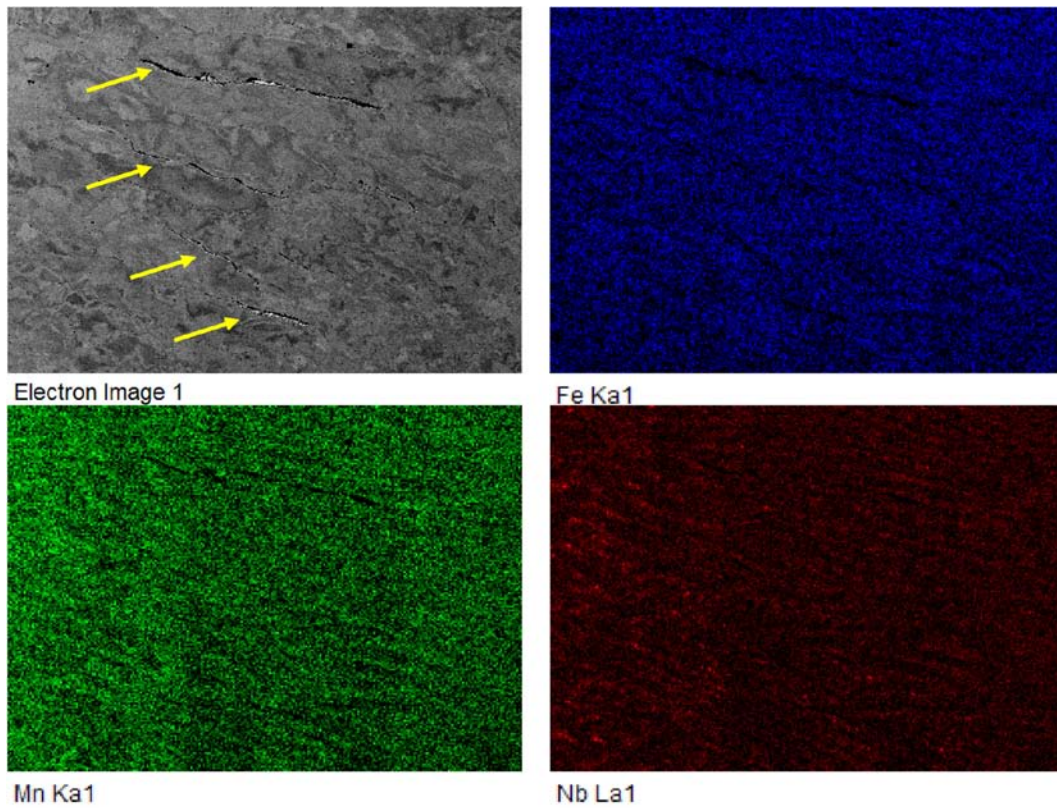


Figure 4.7. SEM-EDS Maps of the MHI Alloy 52 U-groove Mockup Show Very Little Variation in Elemental Composition with the Weld Cracks

4.3 SEM and TEM of Weld Cracks in Alloy 52 – 304SS Overlay Mockup

Selected characterizations have been performed on another overlay mockup containing weld cracks supplied by Pål Efsing of Ringhals. Limited information is currently available on the mockup conditions. However, the Alloy 52 overlay on a stainless steel housing represents a standard welding procedure and the appearance of hot cracks in the mixing (dilution) zone is unexpected. This zone has also been referred to as a sacrificial layer with a non-optimized composition between the 304SS base metal and the Alloy 52 weld metal. An example of the overlay appearance is presented in Figure 4.8 and the two metallographic samples supplied by Ringhals are shown in Figure 4.9.

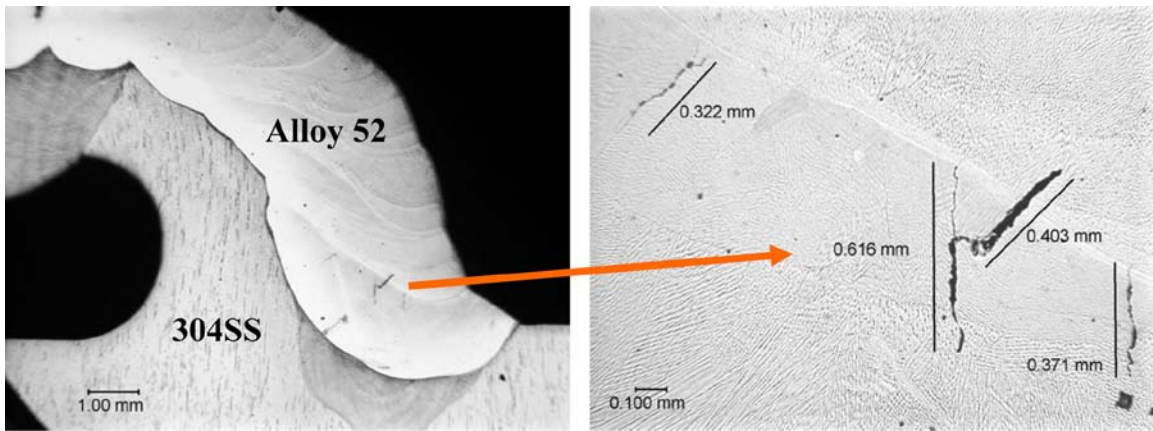


Figure 4.8. Optical Micrographs Provided by Ringhals Showing an Alloy 52 Weld Metal Overlay on a 304SS Housing. An example of a large crack is shown.

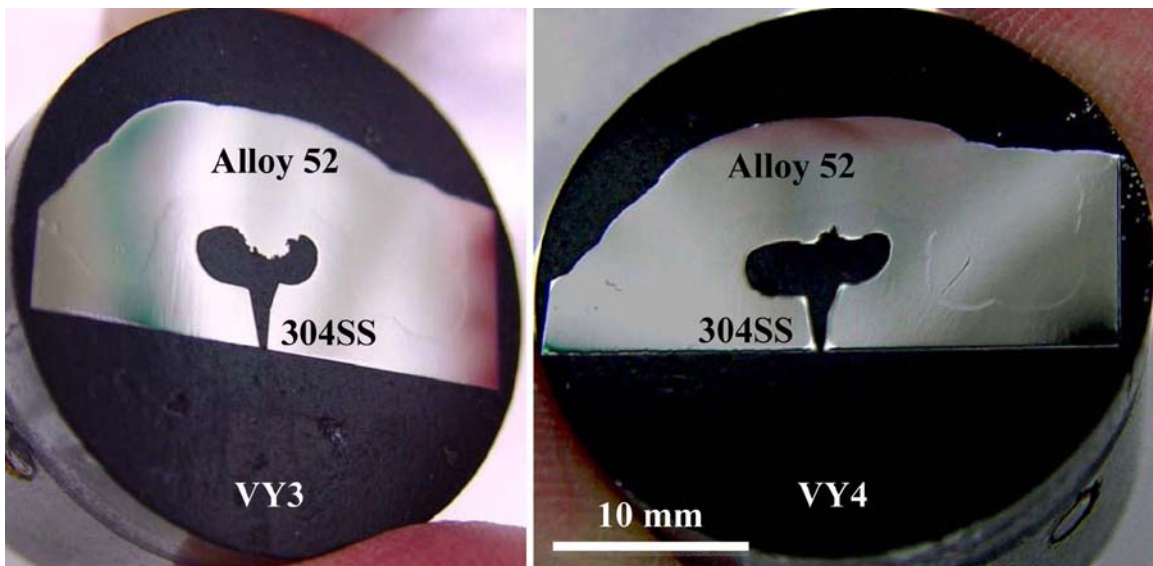


Figure 4.9. Optical Images of As-Received Ringhals Weld Overlays Mounted in Epoxy

Light oxalic etching of the metallographic samples clearly delineated the Alloy 52 weld metal and the 304SS based metal as shown in Figure 4.10. Weld cracks were found in the brighter re-melted regions adjacent to the 304SS, that is, regions identified as A, B, X, and Y. General compositions in these regions were obtained by SEM-EDS and found to be at an intermediate composition between the Alloy 52 and the 304SS. These estimated compositions are listed in Table 4.1 and reveal Fe at levels of 25–36 wt% and Ni levels of 35–46 wt% for regions with hot cracks.

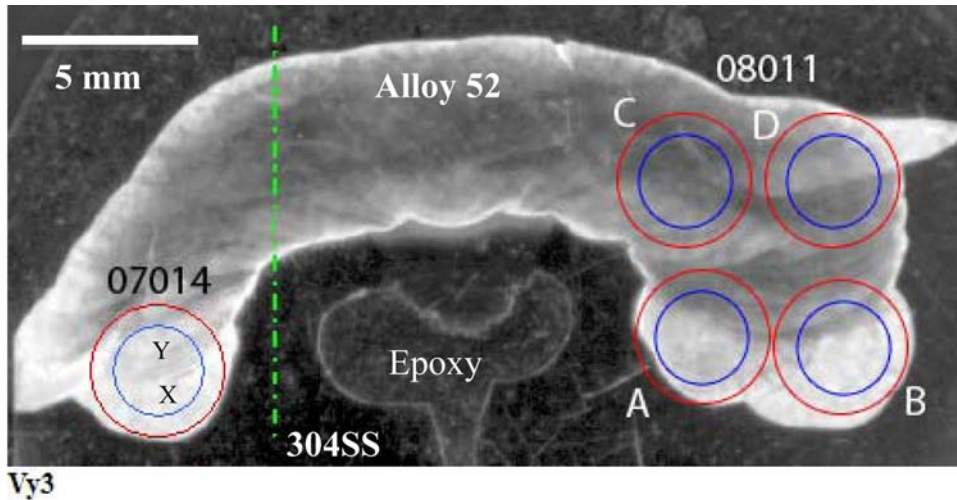


Figure 4.10. Optical Image Providing Overview of the Ringhals Alloy 52 Weld Overlay Sample VY3 After Light Etching and Identifying Various Regions Where TEM Samples were Prepared

Table 4.1. Approximate Region Compositions (wt%) Based on EDS Measurements

	Al	Ti	Cr	Fe	Ni
08011 A	0.46	0.42	27.50	25.01	45.59
08011 B	0.47	0.34	26.93	35.59	36.53
08011 C	0.47	0.46	29.22	19.30	50.46
08011 D	0.65	0.51	29.12	15.81	53.54
07014 X	0.44	0.30	27.41	35.31	35.54
07014 Y	0.36	0.47	28.77	25.16	44.79

Base concentrations for Fe and Ni in Alloy 52 were ~10 and ~60 wt%, while Fe and Ni levels in the 304SS were ~68 and ~8 wt%. Therefore, extensive melting and interdiffusion has occurred during the first overlay passes on the stainless steel resulting in a dilution zone over several millimeters.

An additional example of this dilution zone in relation to the presence of hot cracks is shown by the SEM-EDS map for Fe in Figure 4.11. Several passes are indicated by the change in relative Fe concentration with hot cracks located primarily in the region where the Fe and Ni are nearly equal in composition (30–35 wt%) as measured in Figure 4.12. The microstructural changes in this dilution zone are also dramatic as illustrated in the EBSD image in Figure 4.13. SEM and EBSD images reveal the transition from the fine, equiaxed grains in the 304SS base metal into the large, elongated grains in the melted dilution zone.

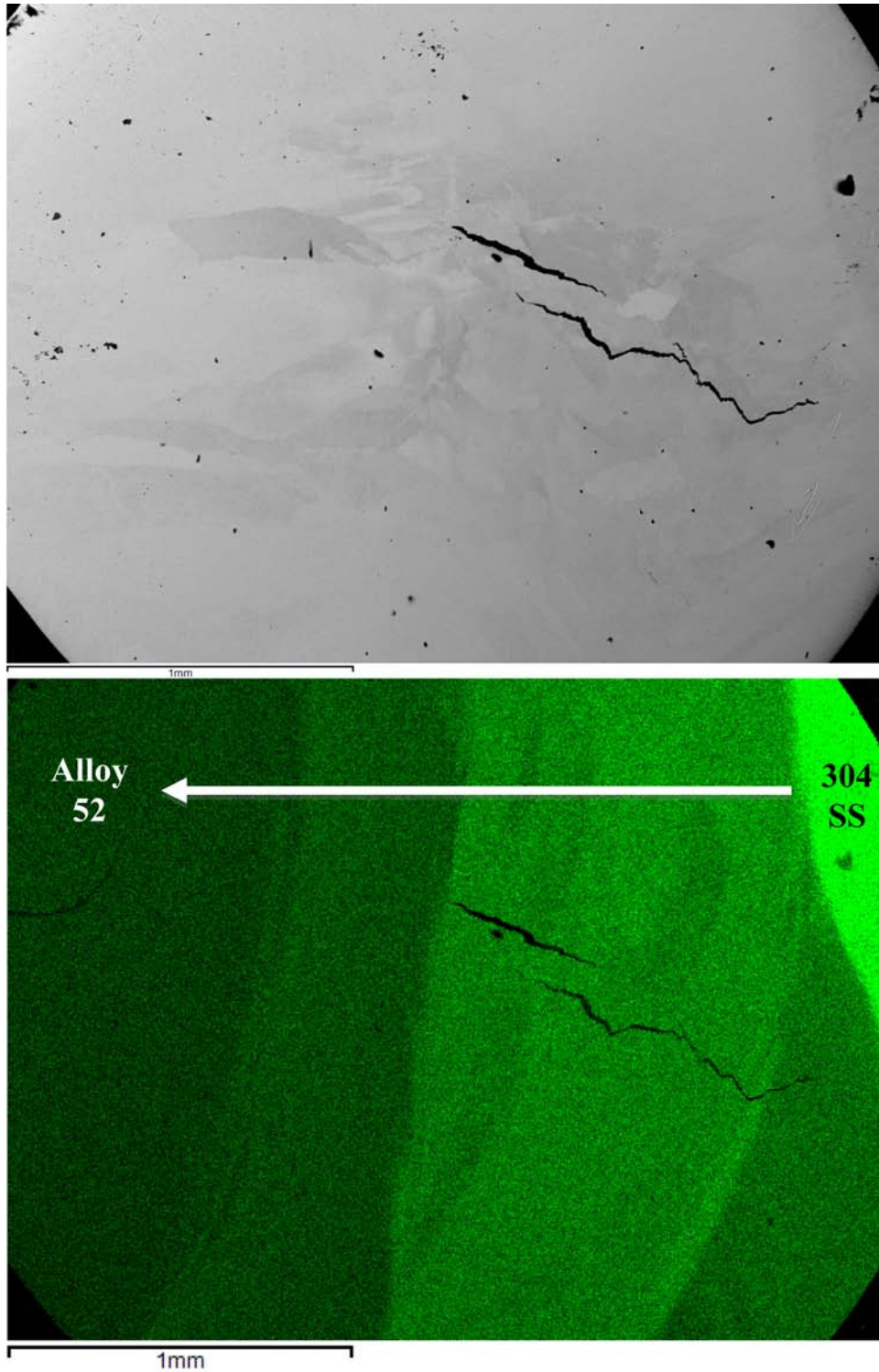


Figure 4.11. SEM and EDS Compositional Map for Fe Illustrating Location of Hot Cracks in the Dilution Layer Between Alloy 52 and 304SS for Overlay Sample VY3

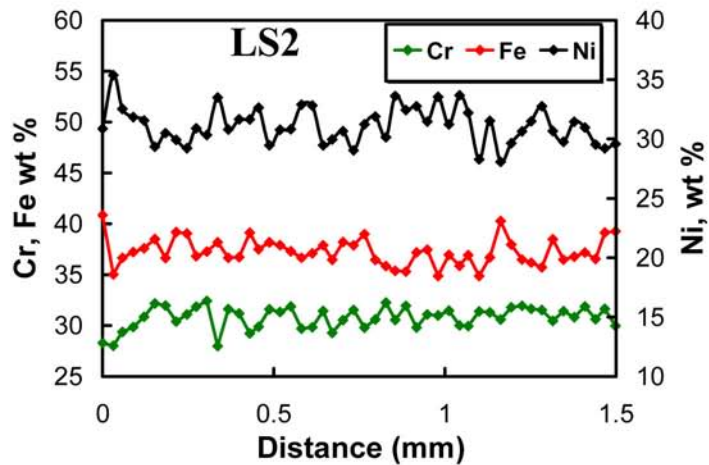
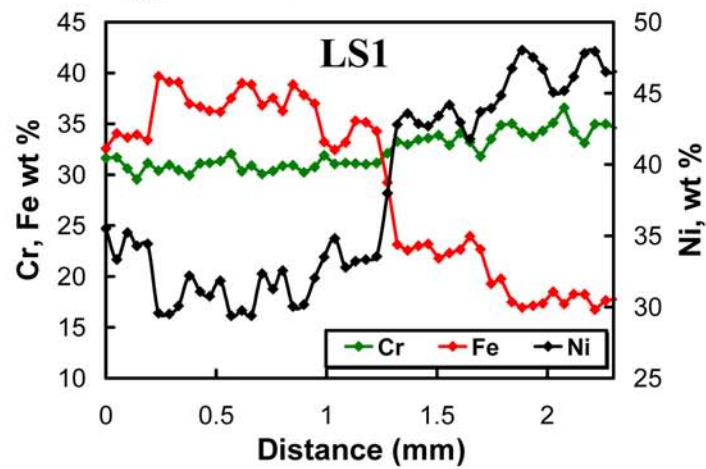
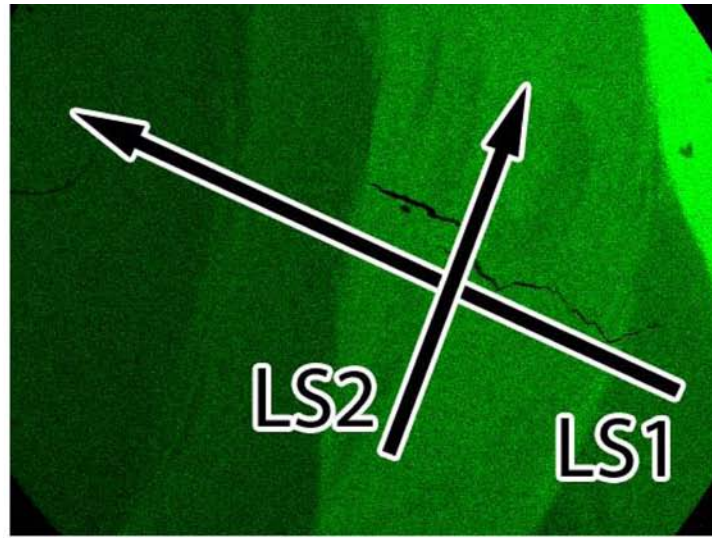


Figure 4.12. Compositional Variation as Measured by SEM-EDS Along the Length and Across a Weld Crack in the Extensive Dilution Zone of the Alloy 52 Overlay

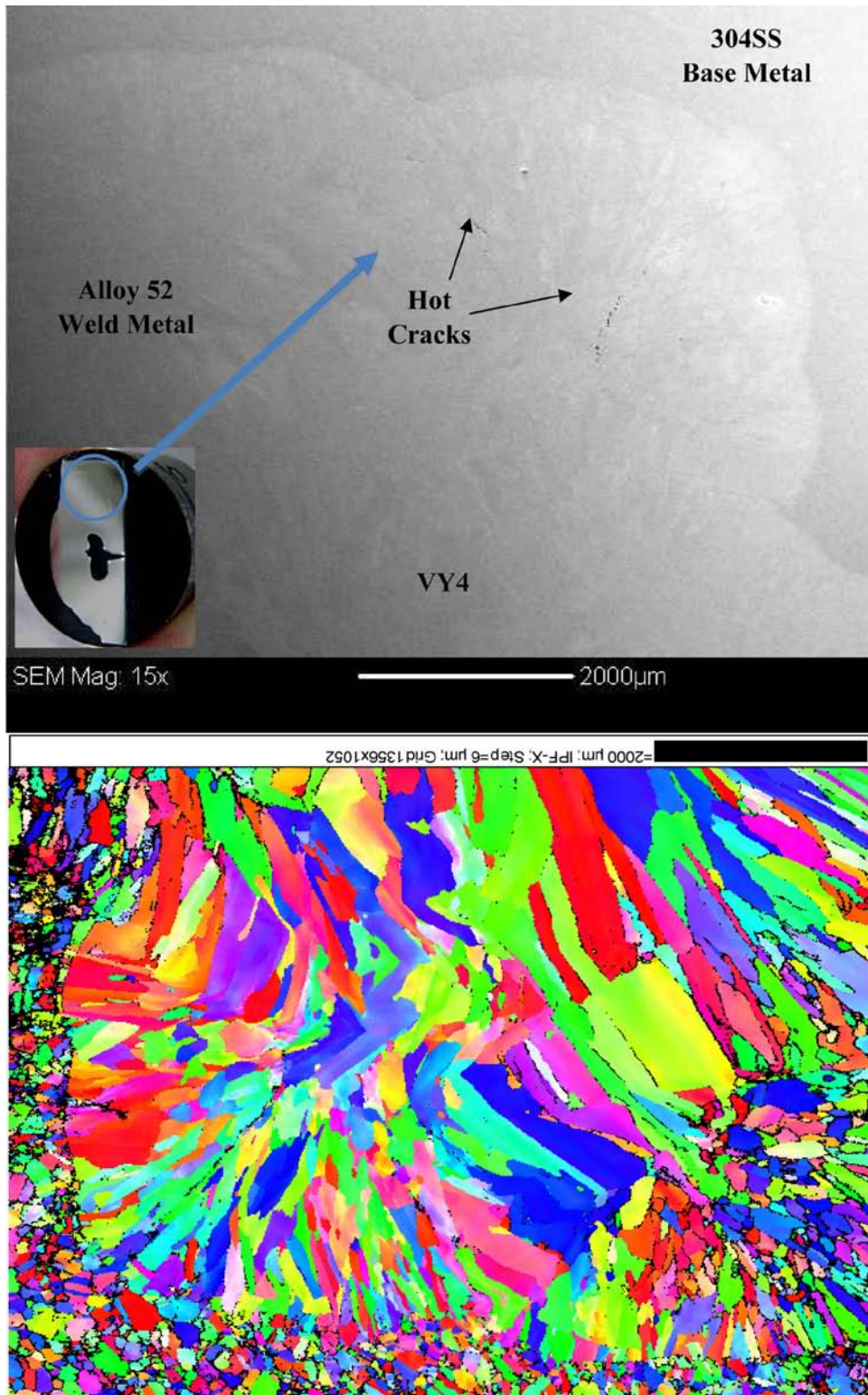


Figure 4.13. SEM and EBSD IPF-X Images Illustrating the Microstructure Across the 304SS Base Metal and Weld Metal Interface Region in Overlay Sample VY4

The next key step in the characterization of the Ringhals overlay samples employed ATEM for the high-resolution examination of grain boundaries and cracks. Transmission electron microscopy (TEM) cross-section samples containing cracks were prepared from the VY3 and VY4 materials by dimple grinding and ion milling. Before cutting and at various times during subsequent preparation, the cracks were protected from contamination during the preparation process by vacuum impregnating the cracks with Gatan G-1 thermosetting resin. Small pieces containing the selected crack regions were cut out and glued to 3-mm-diameter Mo support washers with the targeted features at the centers. After trimming away excess material, the disk samples were flat-ground and finish polished to less than 100 μm total thickness from the non-washed side. The samples were then dimple-ground from the washer side to approximately 15 μm thickness, and briefly ion milled with 5 keV argon ions at $\pm 6^\circ$ incidence to improve the surface finish for SEM examinations. Ion milling was later continued to develop thin areas suitable for TEM analysis, with final milling performed at reduced energy and beam incidence (2 keV, $\pm 4^\circ$) to minimize superficial ion-beam damage. Repeated cycles of ion milling and examination were used to progressively thin the cracks and crack-tip areas for examination. Prior to final thinning for TEM, the finish-polished samples were examined by SEM using backscattered electron (BSE) imaging to observe the cracks and metallurgical grain structures. An example of this documentation is presented in Figure 4.14 and Figure 4.15 from the VY3 material. These observations were used to guide final thinning of regions containing selected cracks and crack tips.

A large number of crack tips have been examined and analyzed from the dilution zone regions of the Ringhals overlay samples VY3 and VY4. All cracks were IG following high-energy grain boundaries containing second-phase precipitates. The most consistent feature at grain boundaries leading the weld cracks was the presence of TiN either as an elongated thin phase or film on the boundary or discrete fine particles. The TEM image and elemental maps in Figure 4.16 highlight the thin elongated Ti-rich phase along a grain boundary leading an IG weld crack. In some locations, the less than 50-nm-thick TiN platelet reaches more than 1 μm in length. Cr-rich M_{23}C_6 carbides are also common at grain boundaries, but tend to be well spaced and nearly spherical.

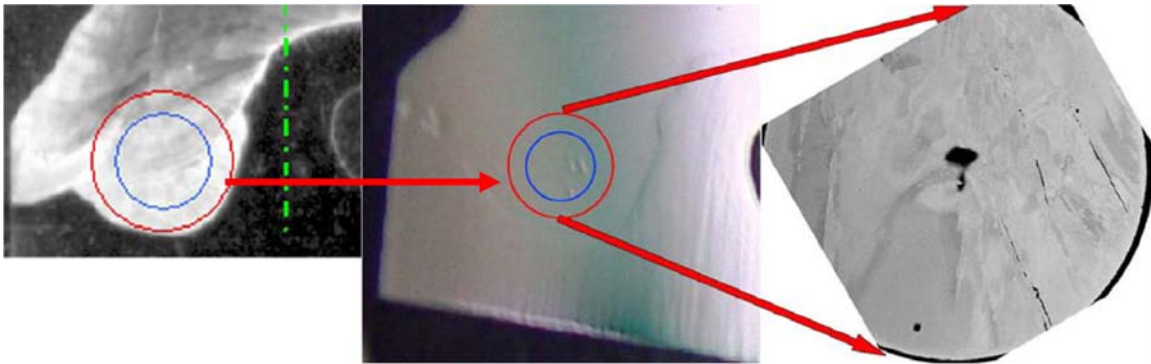


Figure 4.14. Optical and SEM Micrographs Illustrating Region where TEM Sample VY3 Originated in the Original Weld Overlay. The two optical micrographs on the left were obtained using different polishing/etch preparations shown in Figure 4.9 and Figure 4.10.

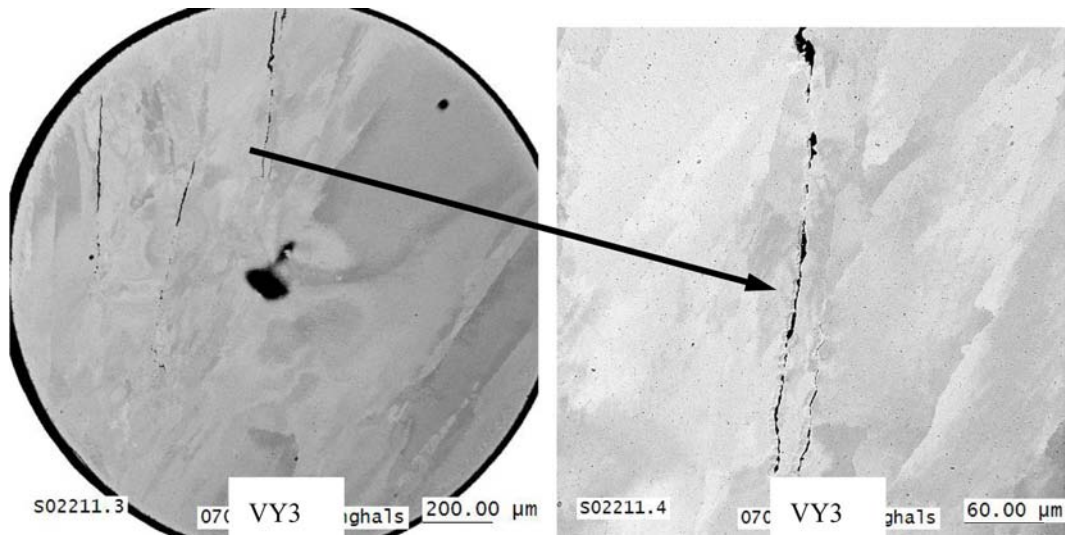


Figure 4.15. Backscatter SEM Images Showing Weld Cracks in Alloy 52 Overlay Sample VY3 and Identifying Region for ATEM Examinations

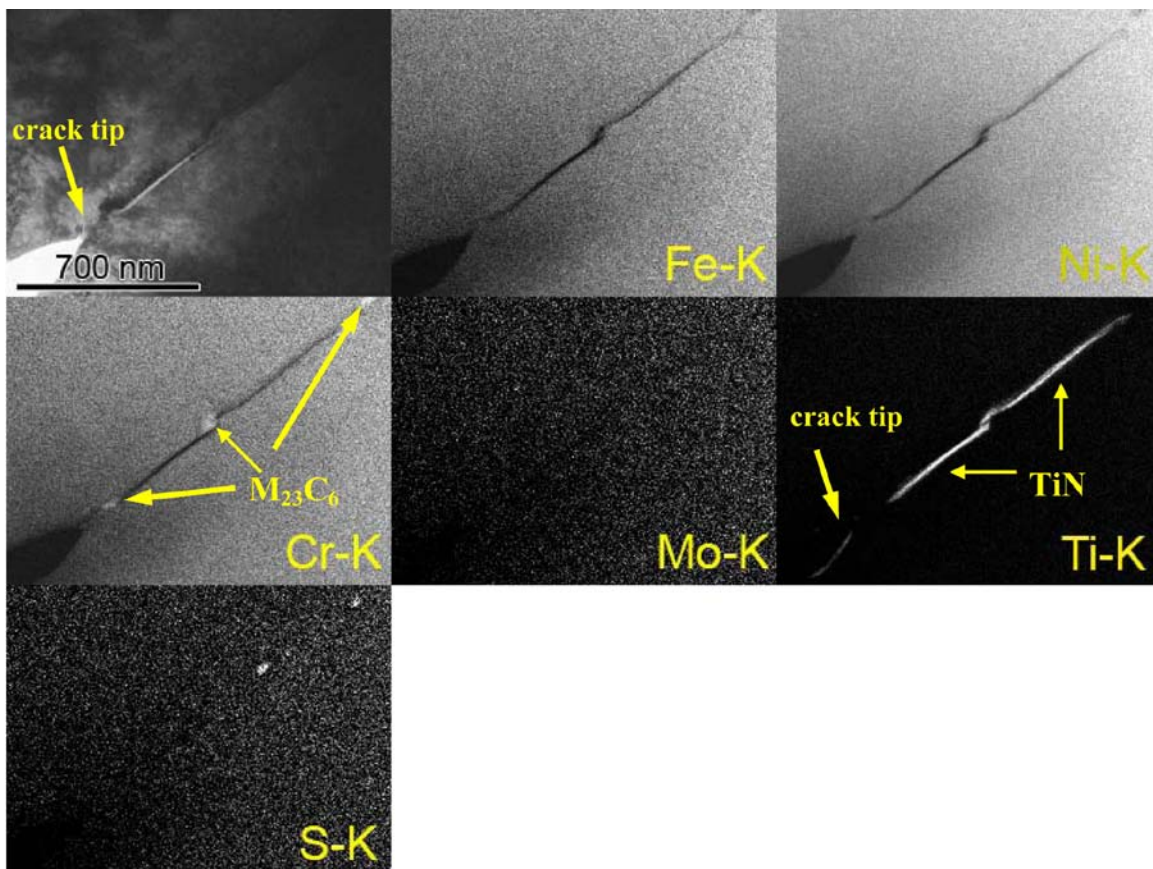


Figure 4.16. TEM Micrograph and Elemental Maps of an IG Crack in Sample VY3. A continuous TiN phase is observed along the grain boundary in front of the crack.

More importantly, the elongated Ti phase has also been found coating one wall of the open crack. This is presented in Figure 4.17, which is higher resolution examination of the same crack tip in Figure 4.16. The Ti compositional map reveals the presence of the 20-nm-thick phase on the lower crack wall suggesting that the crack formed at the Ti precipitate interface during cooling. The crack appears to have stopped at a small $M_{23}C_6$ particle that separates the elongated Ti platelets. Electron diffraction shows that the Ti-rich phase has a MC crystal structure and electron energy loss spectroscopy has clearly indicated that it is a Ti nitride (TiN) and not TiC. Another crack-tip region showing a nearly continuous layer of TiN is illustrated in Figure 4.18. In this section of grain boundary, no $M_{23}C_6$ particles are present but were seen within several microns of this location. Once again, the carbides were more spherical in shape, well spaced along the boundary length and separated by lengths of TiN.

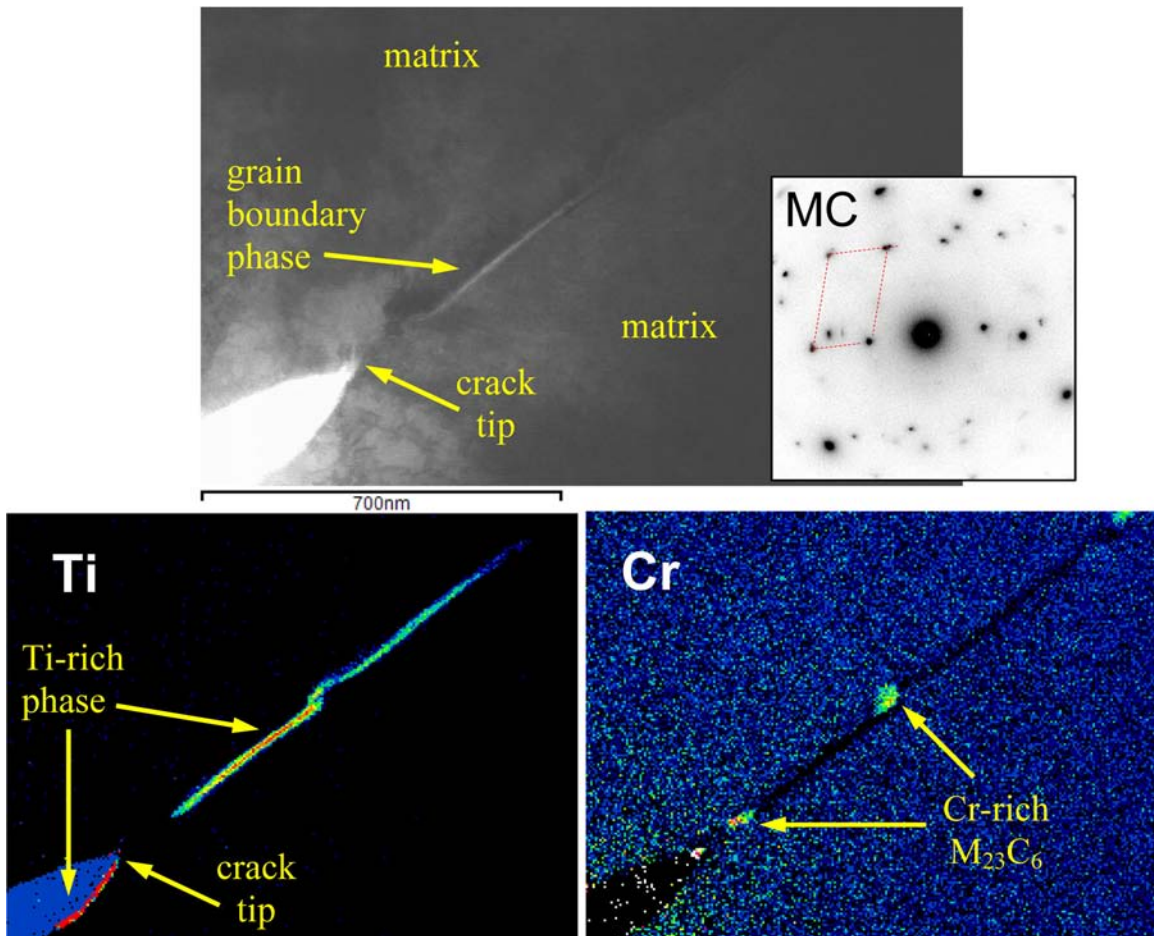


Figure 4.17. Higher Magnification Examination of the Crack-Tip Region Shown in Figure 4.16: (a) TEM bright-field image and selected area diffraction identifying a thin MC-structure second phase; (b) EDS map for Ti demonstrating that the thin phase is highly Ti rich and is located on one side of the crack wall and elongated along the grain boundary; and (c) EDS map for Cr highlighting several IG Cr-rich carbides.

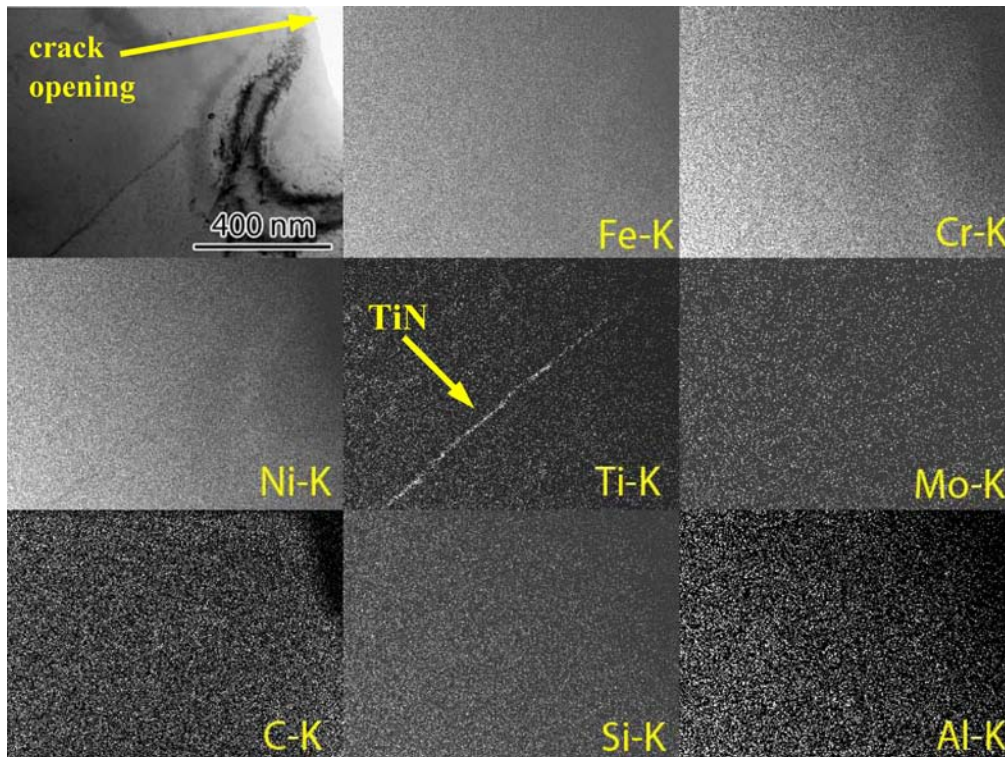


Figure 4.18. Scanning TEM Micrograph and Elemental Maps of a Grain Boundary Leading a Weld Crack in Sample VY3. A nearly continuous TiN phase is observed along the grain boundary in front of the crack. The crack opening appears large and rounded due to repetitive ion milling to thin the grain boundary region in front of the crack.

One final example of a grain boundary leading a weld crack is presented in Figure 4.19. In this case, two weld cracks were found along the same grain boundary with a small section ($\sim 0.6 \mu\text{m}$) of non-cracked material that could be analyzed. TiN was again discovered along the grain boundary, but as a high density of fine particles and not as an elongated thin phase. A single, M_{23}C_6 carbide can be seen within the boundary length as well.

Various TEM examinations were also performed in regions of the weld outside of the dilution zone and away from the regions with weld cracks. While grain boundary microstructures varied, the most significant difference appeared to be the distribution of TiN particles. Isolated particles were occasionally identified on boundaries with a moderate density of M_{23}C_6 carbides, but a continuous IG phase was only found associated with the dilution zone and the weld cracks. Based on these observations, grain boundary TiN precipitation is believed to play an important role in the cracking during weld solidification for this Alloy 52 overlay on 304SS.

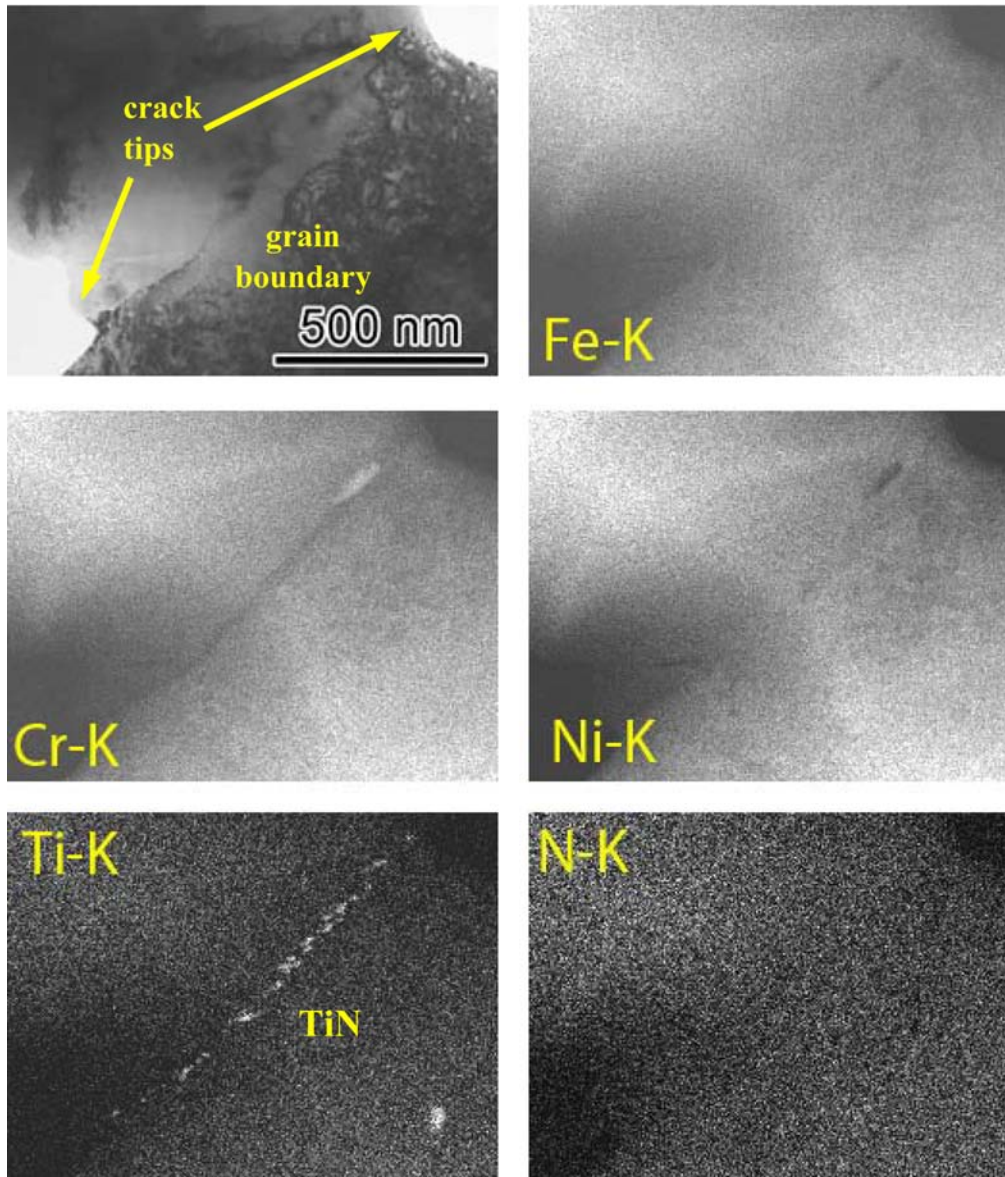


Figure 4.19. EDS Elemental Maps Illustrating Small TiN_2 Particles and One Large M_{23}C_6 Carbide Along a Grain Boundary Along the Path of a Hot Crack. Nitrogen cannot be detected in the TiN particles by EDS mapping because of the weak N-K signal.

4.4 SEM of MHI Alloy 152 Weld Mockup

General microstructural examinations were performed on the MHI Alloy 152 weld mockup as part of NRC project JCN N6007. No attempt was made at that time to look for weld defects or cracks. The purpose was to document the general microstructure in the general regions where SCC crack-growth testing would be performed. An indication of the dendritic microstructure is presented in Figure 4.20.

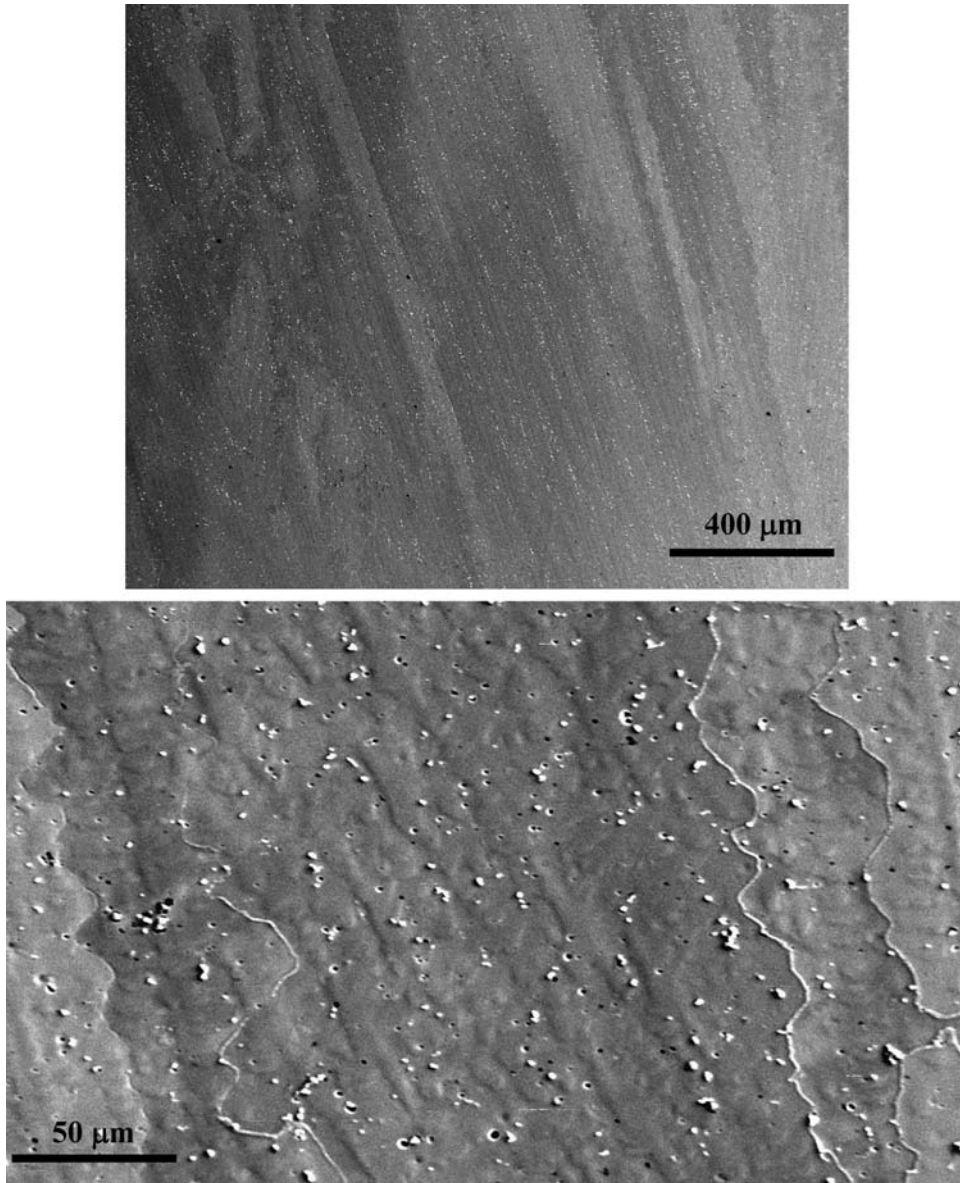


Figure 4.20. SEM-SE Images Illustrating Dendritic Large Grain Microstructure in the MHI Alloy 152 Weld Metal. Higher magnification (lower image) shows high density of second phase particles.

Three-mm disc samples for TEM were prepared and microstructures examined. Characterization revealed that many of the dendritic grain boundaries contain a widely varying distribution of metal carbides. Figure 4.21 and Figure 4.22 illustrate the variability along the different boundaries in the weld metal. Both $M_{23}C_6$ and MC carbides were found on boundaries and appear to precipitate independent of each other. In Figure 4.21, a larger Cr-rich $M_{23}C_6$ carbide was identified along with numerous small NbC particles. $M_{23}C_6$ and MC carbides are seen to precipitate in an interspaced pattern on the grain boundary in Figure 4.22.

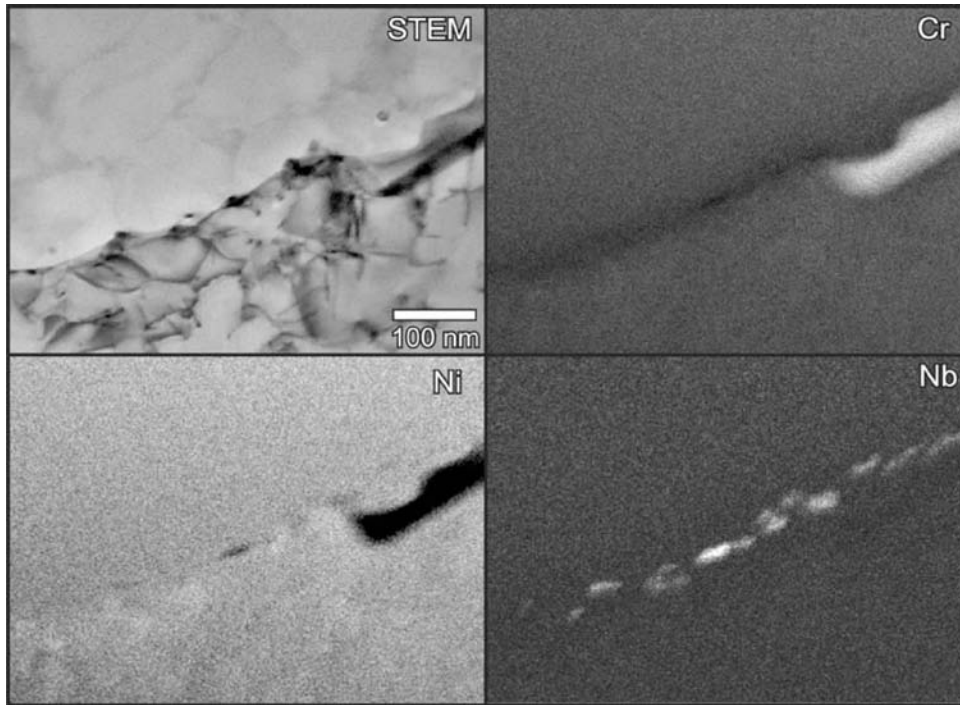


Figure 4.21. Grain Boundary Showing a Single Large Cr-carbide with Numerous Smaller Nb-Ti Carbides. In this case, no Ti was found associated with the Nb MC carbides.

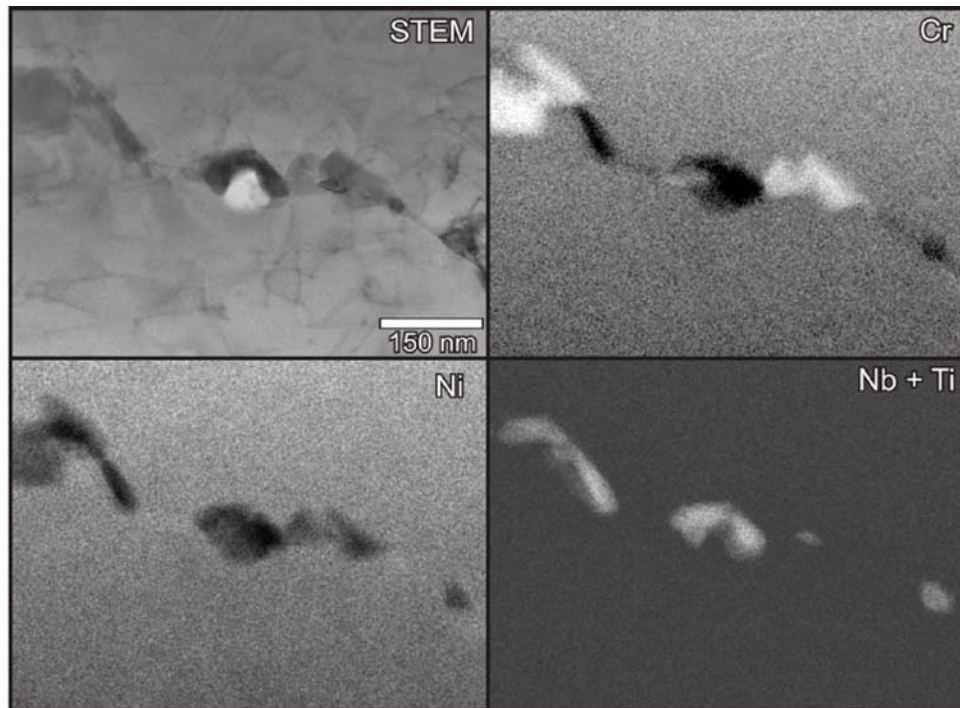


Figure 4.22. Compositional Maps Taken in STEM Mode Revealed that Both Cr-rich and Nb-rich Carbides are Present on the Boundary Between Two Dendrites. The MC carbides contained both Nb and Ti.

SEM examinations were performed on samples cut from the edge of the MHI Alloy 152 weld in the “transition region” from the 304SS to the buttering to the main weld. A dilution zone was created between the Fe-base 304SS and the butter passes to the Ni-base Alloy 152 material. This region was of interest because compact tension samples were machined to evaluate SCC crack-growth response of this interface as shown in Figure 4.23. As expected, the face-centered-cubic austenite phase was present throughout the transition region and colonies of ferrite were identified near the weld interface.



Figure 4.23. Photograph Illustrating the Location of Two CT Specimens that were Machined with the Crack Plane Coincident with the 304SS – Alloy 152 Weld Fusion Line

The optical and SEM images in Figure 4.24 illustrate the changing microstructure across the transition region. The chromium-rich colonies of ferrite were noted only on the base-metal side of the weld, extending up to ~50 μm from the weld interface. Note that these isolated ferrite colonies surrounded by austenite were not continuous along the weld interface. Hardness measurements revealed only minor changes in hardness across the transition zone, with a small increase in hardness in the ferrite colonies (~260 in the ferrite colony vs. ~230 in base metal and weld, Vickers hardness at 100 gf load). The austenite varies considerably in composition from a Ni-rich austenite in the weld region to Fe-rich austenite in the stainless steel base metal. EDS maps are shown in Figure 4.25, while a representative compositional profile across the transition region is provided in Figure 4.26. The Cr-rich ferrite near the weld interface can be identified along with the Ni and Cr varying considerably across the transition region, and the Fe and Ni fluctuating within the weld region.

In comparison to the Alloy 52 overlay material discussed in the previous section, the dilution zone with the stainless steel is quite narrow. A sharp increase in Ni concentration can be seen over an approximately 10- μm distance reaching more than 50 wt%.

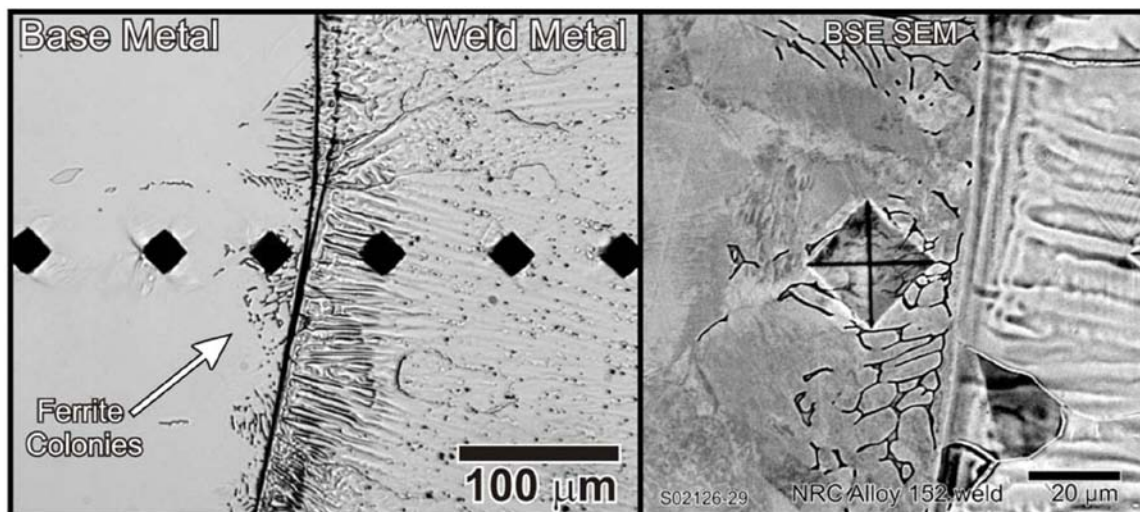


Figure 4.24. Left Image Shows an Optical Micrograph of the Transition Region with the Hardness Indentation Measurements. The hardness changed very little over the entire region despite the significant differences in microstructure.

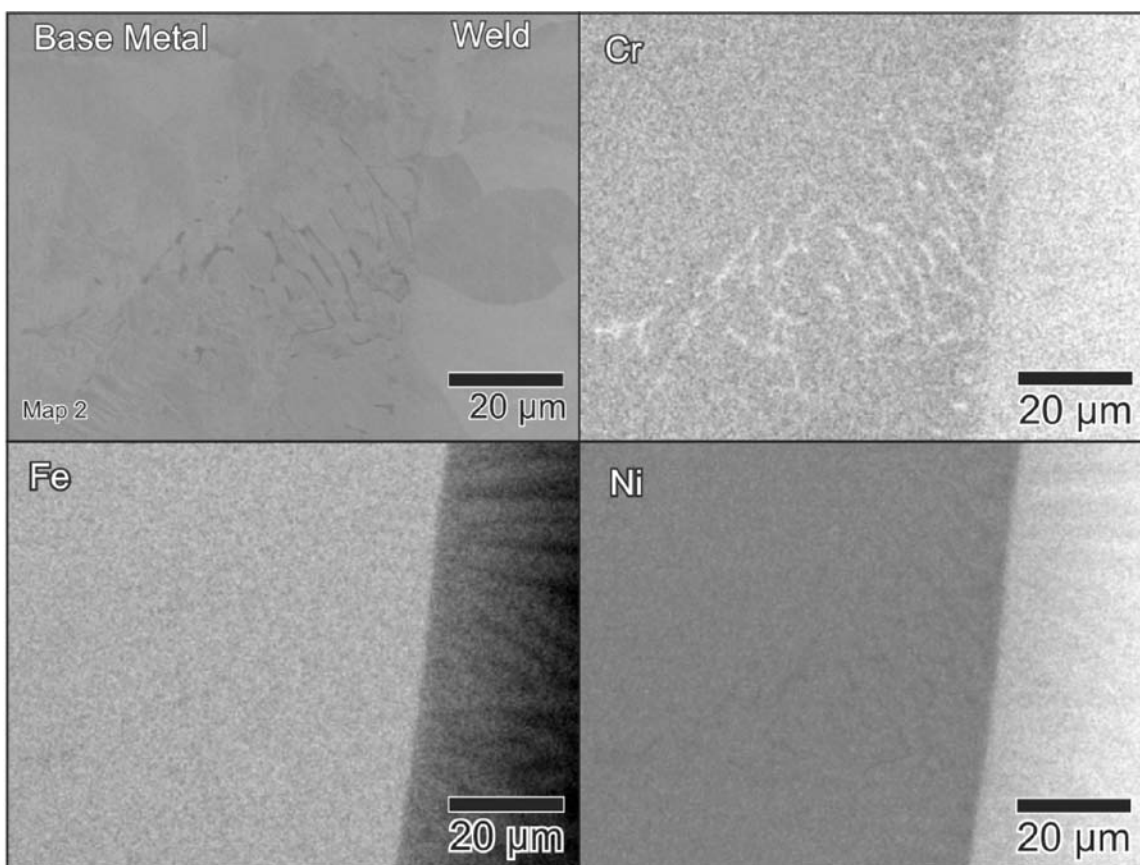


Figure 4.25. Compositional Map Taken Over the Alloy 152 – 304SS Interface

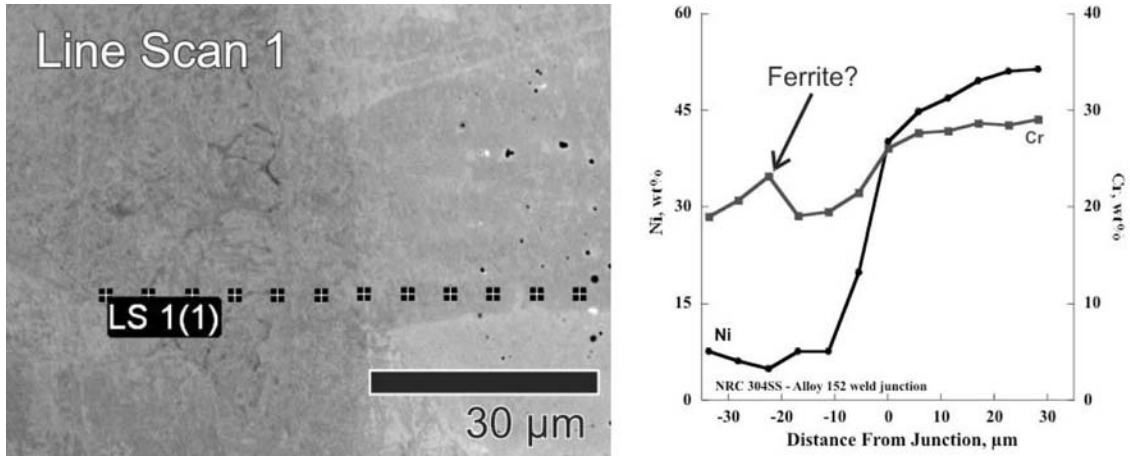


Figure 4.26. The Line Profile Across the Transition Region Shows that the Ni Changes from ~8 wt% in the Base Metal to ~50% in the Nearby Weld Region. The Cr change is smaller, decreasing from ~29% in the weld to ~19% in the 304SS austenite phase. The small spike in Cr concentration on the base metal side may be due to a ferrite colony.

5.0 Summary of Preliminary Results

The primary goal of these initial examinations was to assess defects in prototypic, industry-produced, Alloy 52 and 152 mockup welds. As described in Section 2.0, weld metals were characterized in three different structures: (1) Alloy 52 and 152 U-groove weld mockups, (2) an Alloy 52 M overlay, and (3) an Alloy 52M inlay mockup. The only significant defects identified within the Alloy 52, 52M, or 152 welds were IG cracks. No evidence for other weld defects was found.

The optical appearance of the weld cracks did not vary significantly between the four different mockups. Crack openings varied from less than 1 μm and almost invisible to up to approximately 10 μm . Short cracks appear to have approximately the same amount of crack opening as the longer cracks. The size and appearance of the cracks may have been affected by the preparation method. As noted, simple metallographic polishing to a 1- μm finish was performed. It is possible that short, tight cracks could be obscured and difficult to identify with this preparation method. Information on the length of the cracks along the weld-pass direction was desired, but the distance between slices was too large to obtain meaningful data. Serial polishing would be required to assess the three-dimensional aspect of the observed cracks.

General differences among the various welds were observed in both the location and density of weld cracks. The fewest cracks were identified in the Alloy 152 weld metal, either in the butter layers or the fill. A sharp macroscopic crack in the Alloy 152 was present at the base of the U-groove weld extending from the initial 304SS plate and butter butt joint. Even for this high-stress location, only a single secondary crack was present in this region (quite different than for the Alloy 52 weld). The two other confirmed weld cracks in the Alloy 152 U-groove mockup were near the top of the weld and near the butter interface off to one side of the weld. Therefore, the Alloy 152 weld was quite resistant to the formation of weld cracks whether due to the weld metal composition or to the welding procedure or both.

The MHI Alloy 52 U-groove mockup revealed a substantial amount of weld cracks clustered around the main macroscopic crack that ran up into the fill weld from the 304SS plate and butter butt joint. This main crack was much more open than seen in the Alloy 152 weld indicating much higher local stresses. Although this local region showed a high density of cracks, it is important to note that no other cracks were found in the Alloy 52 weld. As a result, the Alloy 52 in the U-groove weld also appears to be resistant to the formation of cracks except in the high stress region created above the plate butt joint.

The greatest number of weld cracks was found in the Ringhals Alloy 52M overlay. They were clustered in three local regions on both cross-section slices examined. It is uncertain whether this distribution is random or there were differences in the weld wire or practice local to these regions. Because the Alloy 52M layer was robotically welded, one would expect the welding parameters to have remained constant. The majority of the weld cracks appeared to be randomly placed in each of the three sections, but there were many small weld cracks associated with the first Alloy 52M weld pass near the Alloy 690 interface. This local grouping was identified in section 8 of the front face and section 1 of the back face. There were also a few instances of small weld cracks at or near the final Alloy 52M weld pass in section 8 of the back face slice. These results suggest that the Alloy 52M overlay weld metal is more susceptible to the formation of IG cracks during welding. Additional characterization activities in the

three sections containing a high density of weld cracks are warranted along with discussions with Ringhals concerning possible reasons for the enhanced local cracking.

The final mockup examined was the Ringhals Alloy 52M inlay. Most of the weld cracks were found near the final Alloy 52M weld pass in this rather thick inlay. Only isolated cracks were identified near the Alloy 52M – Alloy 82 interface, and nearly all of these were in the Alloy 82 material. The weld cracks in the Alloy 52M were typically less than 100 μm in length, but there was one possible instance of an approximately 500- μm crack in the final weld pass. There is insufficient information to determine whether these cracks formed during the application of the Alloy 52M inlay mockup by Ringhals or whether they were formed during the application of the final Alloy 152 overlay by Westinghouse. Further characterization of the Alloy 52M cracks would be useful; however, the Alloy 52M overlay was resistant to the formation of weld cracks.

Attempts were made to quantify aspects of the metallographic results for the weld cracks. Overall observations of the weld cracks indicate a relatively low density of small cracks generally less than 100 μm in length. For all but the MHI Alloy 152 weld, a sufficient number of cracks were found to permit measurement of crack length density and length distribution plots. The areal number density versus size distribution for the Alloy 52M overlay material is shown in Figure 5.1. The peak in the weld crack length is approximately 25 μm with the number density falling off rapidly as the weld crack length increases. The areal density of the Alloy 52M inlay mockup is shown in Figure 5.2. As with the overlay, the crack length peaks at approximately 25 μm with the distribution tailing off to a very low density of longer cracks, almost 0.5 mm in length. The density of cracks in the inlay is approximately one third of the overlay for the 25- μm -size range, but only slightly lower density for cracks longer than 25 μm . The areal number density versus crack length of the MHI Alloy 52 slice is shown in Figure 5.3. Although the weld cracks were isolated to the region around the large macroscopic weld crack that grew from the base of the U-groove, the entire area of the slice was used to calculate the areal number density. Based on this area, the density of cracks in the MHI Alloy 52 U-groove weld is approximately one-half the density of cracks in the Ringhals overlay mockup. If the area used in the calculation is confined to the region around the macroscopic crack, then the number density would increase approximately by a factor of 10. The density of cracks in the MHI Alloy 152 mockup was too low to obtain a statistically relevant size distribution of cracks. The total areal number density of cracks was less than 0.05 cm^{-2} with cracks no longer than 300 μm .

Based on the preliminary weld crack examinations reported here, brief comments can be made on implications to the use of thin, high-Cr overlays or inlays to provide corrosion resistance. The first issue is whether the observed cracks provide a continuous path for water to reach the more SCC-susceptible lower Cr material. While the typical crack size in all the welds was 100 μm or less, in three of the weld mockups, several 500- μm -long cracks were observed. This length is insufficient for a single crack to span even a thin overlay, but a clustering of interconnected cracks may potentially provide a path through a thicker weld metal layer. This seems unlikely based on the current limited results; however, more detailed studies of crack size and three-dimensional distributions would need to be performed to better assess the probability that such interconnected cracks could exist.

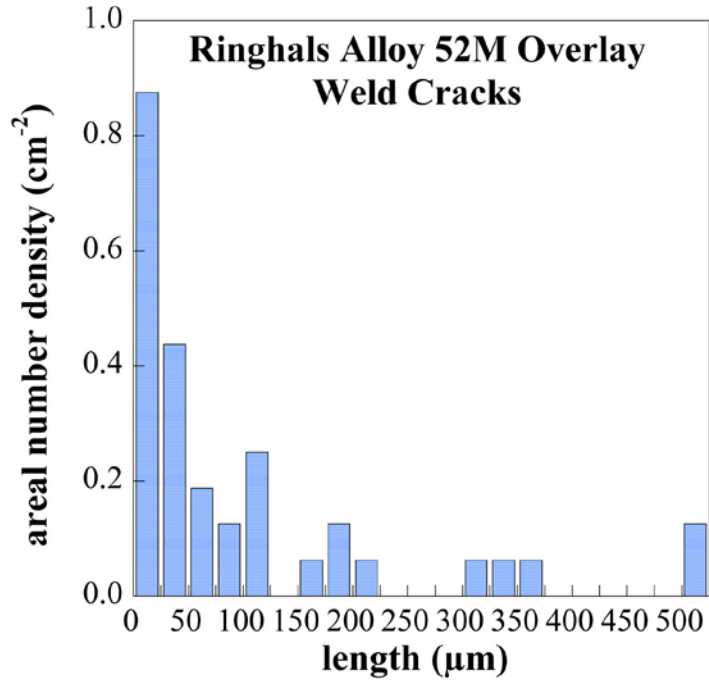


Figure 5.1. Areal Number Density Versus Crack Length for the Weld Cracks Observed in the Ringhals Alloy 52M Overlay Mockup

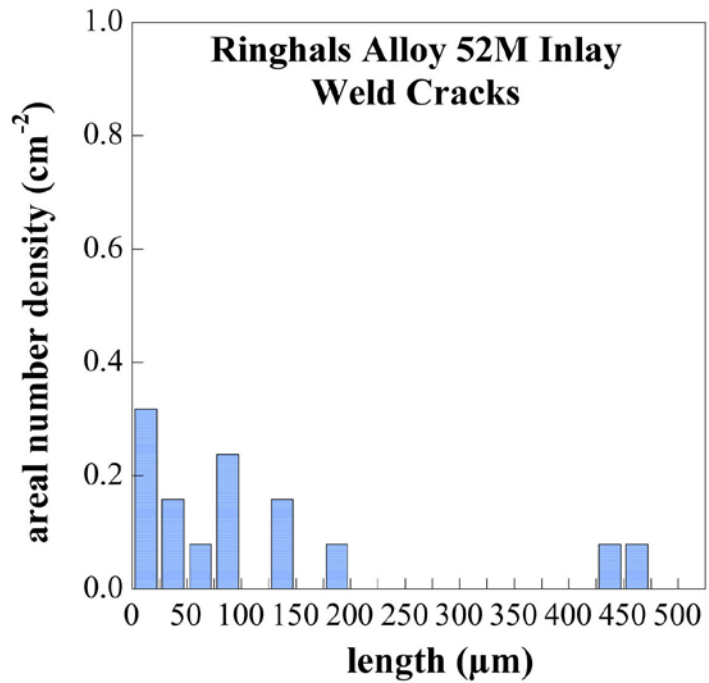


Figure 5.2. Areal Number Density Versus Crack Length for the Weld Cracks Observed in the Ringhals Alloy 52M Inlay Mockup

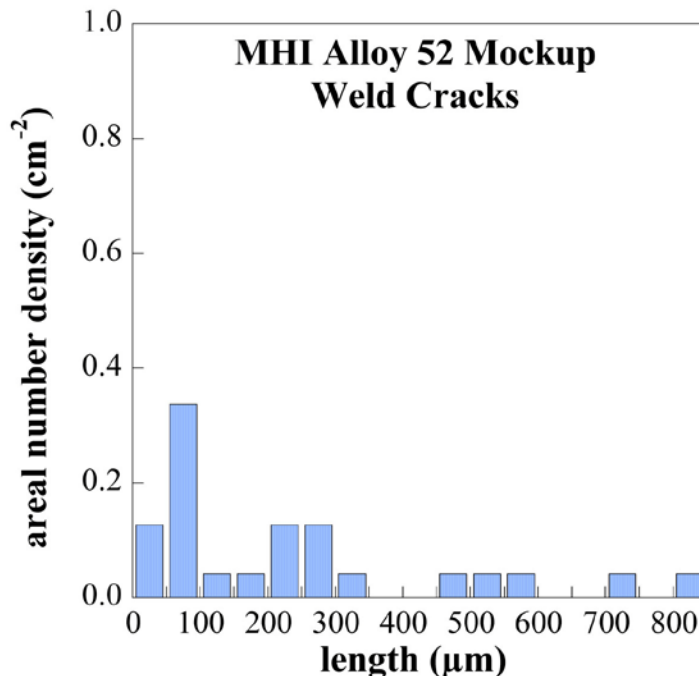


Figure 5.3. Weld Crack Areal Number Density Versus Length Observed in the MHI Alloy 52 U-groove Mockup. Although the weld cracks were isolated to the region around the large macroscopic weld crack, the entire area of the slice was used to calculate the areal number density.

More importantly, these pre-existing flaws can act as sites for crack growth during LWR service. The location and length of a weld crack in the inlay or overlay would obviously have a strong affect on the local stress intensities. A long weld crack that intersects the surface of an inlay or overlay would be subject to the highest fatigue-driven stress and clusters of cracks could be more easily interconnected. Similar issues can be envisioned for a weld crack on the surface acting as a nucleation site for the growth of an SCC crack. Measured SCC propagation rates of these materials are extremely slow, with perhaps a maximum rate of approximately 0.1 mm/year at relatively high stress intensity values. It would take roughly 20 years for an SCC crack to span a 2-mm-thick inlay repair. A key issue is whether the microstructure in the regions of weld cracks is inherently more susceptible to SCC. This could result from local deformation-induced structures, segregation-induced microchemistries, or second-phase precipitation particularly associated with grain boundaries where pre-existing cracks are present. Focused SCC testing has not been performed to evaluate such microstructural/microchemical variations in candidate inlay and overlay materials. In fact, high-resolution characterizations of these weld metals have been extremely limited with the most pertinent work done by George Young at Knolls Atomic Power Laboratory.

Additional research is needed to better understand the formation of weld cracks and their potential effects on subsequent LWR component reliability in service. Characterization of these (and other) weld mockups to a greater level of detail could help answer some of these questions. Further SEM and ATEM examinations of cracked and uncracked grain boundaries would be helpful in understanding the root cause of the cracking. It could provide some information about compositional changes that may affect subsequent SCC crack growth in regions of a material where many weld cracks are present. Information

obtained from this study could also serve in part to help guide the development of more crack-resistant, high-Cr weld metals. Interactions with George Young continue and may enable access to unique, well-controlled Alloy 52 weld metals with hot cracks for study. This would include both characterizations and SCC crack-growth testing. Beyond these higher-resolution examinations and SCC testing, serial polishing could also be performed to provide information about the length of these cracks along the welding direction and the three-dimensional structures for the clustered cracks. As noted above, this information would be required to assess the likelihood of weld cracks linking to create a continuous path through a thin inlay or overlay.



Pacific Northwest
NATIONAL LABORATORY

*Proudly Operated by **Battelle** Since 1965*

902 Battelle Boulevard
P.O. Box 999
Richland, WA 99352
1-888-375-PNNL (7665)

www.pnl.gov



U.S. DEPARTMENT OF
ENERGY